Rab6 Coordinates a Novel Golgi to ER Retrograde Transport Pathway in Live Cells✪

Jamie White,*‡ Ludger Johannes,§ Frédéric Mallard,§ Andreas Girod,‡ Stephan Grill,*‡ Sigrid Reinsch,‡ Patrick Keller,‡ Barbara Tzschaschel,‖ Arnaud Echard,§ Bruno Goud,§ and Ernst H.K. Stelzer*‡

*Light Microscopy Group and ‡Cell Biophysics and Cell Biology Programme, European Molecular Biology Laboratory, Meyerhofstrasse 1, D-69117 Heidelberg, Germany; §Laboratoire Mécanismes moléculaires du transport intracellulaire, Institut Curie, CNRS UMR 144, Paris, Cedex 05, France; and ‖GBF-National Research Institute for Biotechnology, Department of Microbiology, Mascheroder Weg 1, 38124 Braunschweig, Germany

Abstract. We visualized a fluorescent-protein (FP) fusion to Rab6, a Golgi-associated GTPase, in conjunction with fluorescent secretory pathway markers. FP-Rab6 defined highly dynamic transport carriers (TCs) translocating from the Golgi to the cell periphery. FP-Rab6 TCs specifically accumulated a retrograde cargo, the wild-type Shiga toxin B-fragment (STB), during STB transport from the Golgi to the endoplasmic reticulum (ER). FP-Rab6 TCs associated intimately with the ER, and STB entered the ER via specialized peripheral regions that accumulated FP-Rab6. Microinjection of antibodies that block coatomer protein I (COPI) function inhibited trafficking of a KDEL-receptor FP-fusion, but not FP-Rab6. Additionally, markers of COPI-dependent recycling were excluded from FP-Rab6/STB TCs. Overexpression of Rab6:GDP (T27N mutant) using T7 vaccinia inhibited toxicity of Shiga holotoxin, but did not alter STB transport to the Golgi or Golgi morphology. Taken together, our results indicate Rab6 regulates a novel Golgi to ER transport pathway.

Key words: intracellular transport • Shiga toxin • Rab6 protein • KDEL receptor • green fluorescent protein

Anterograde transport along the exocytic pathway is the flux of proteins and lipids from the ER through the Golgi apparatus to their final destination in an intracellular compartment, such as the endosomes, or to the plasma membrane. Retrograde transport along the exocytic pathway is the flux of proteins and lipids from later to earlier exocytic compartments, reversing the order of organelle entry with respect to the anterograde transport.

Retrograde transport from the Golgi to the ER retrieves ER resident proteins that have escaped with the anterograde flux (Pelham, 1991). Such retrieval depends on specific signals: soluble ER resident proteins rely on the consensus sequence KDEL at their COOH terminus (Munro and Pelham, 1987; Pelham, 1988), and transmembrane ER resident proteins rely on signals in their cytosolic tails (Jackson et al., 1990; Schutze et al., 1994). Transport mediated by these retrieval signals depends on the coatomer protein I (COPI)[1] cytosolic coat complex (Cosson and Letourneur, 1994; Letourneur et al., 1994; Aoe et al., 1997). Recruitment of COPI to membranes is mediated by the small GTPase ADP-ribosylation factor-1 and its effectors (Palmer et al., 1993; Aoe et al., 1997) and presumably regulates the formation of retrograde transport carriers (Cosson and Letourneur, 1997). In addition to ER resident proteins, signal-mediated, COPI-dependent mechanisms account for the retrograde transport of a class of transmembrane proteins (the p24 family) that localize primarily to the Golgi (Stamnes et al., 1995; Sohn et al., 1996; Dominguez et al., 1998; Füllekrug et al., 1999). The p24 proteins contain cytosolic retrieval motifs (Stamnes et al., 1995) which bind COPI coatomer in vitro (Dominguez et al.,

✪The online version of this article contains supplemental material.

Drs. Goud and Stelzer are principal investigators.

Drs. White and Johannes contributed equally.

Address correspondence to Jamie White, Light Microscopy Group and Cell Biophysics and Cell Biology Programme, European Molecular Biology Laboratory, Meyerhofstrasse 1, D-69117 Heidelberg, Germany. Tel.: 49 6221 387 123. Fax: 49 6221 387 306. E-mail: jwhite@embl-heidelberg.de

Dr. Reinsch's present address is Gravitational Research Branch, NASA Ames Research Center, M/S 239-11, Moffett Field, CA 94035-1000.

1. *Abbreviations used in this paper:* CFP, cyan fluorescent protein; CLSM, confocal laser scanning microscopy; COP, coatomer protein; CT, Cholera toxin; ER, endoplasmic reticulum; GFP, green fluorescent protein; KDELR, KDEL-receptor; PE, *Pseudomonas* exotoxin A; ST, Shiga toxin; STB, Shiga toxin B-fragment; TCs, transport carriers; YFP, yellow fluorescent protein.

1998; Schröder-Köhne et al., 1998; Stamnes et al., 1995), presumably allowing these proteins to cycle transiently to the ER. Thus, ER retrieval defines a general signal-mediated, COPI-dependent pathway of retrograde transport from the Golgi to the ER, and not simply a mechanism for localization of ER resident proteins.

In addition to cellular proteins, certain toxin proteins undergo retrograde transport to the ER (Sandvig and van Deurs, 1996; Johannes and Goud, 1998; Lord and Roberts, 1998). Toxins of the AB-toxin family, which include cholera toxin (CT), Shiga or Shiga-like toxins (SLT or verotoxins), and *Pseudomonas* exotoxin A (PE), bind to the cell surface and are transported from the plasma membrane via the Golgi to the ER (Sandvig et al., 1992; Majoul et al., 1996; Johannes et al., 1997). Binding of these toxins is mediated by the nontoxic B-fragment, which can undergo retrograde transport independent of the toxic A subunit (Sandvig et al., 1994; Johannes et al., 1997). Because they can be purified and added exogenously to cells, retrograde transport of toxin proteins is initially unidirectional, in contrast to the recycling behavior of ER residents, KDEL-receptor (KDELR), or p24 proteins, thus allowing observation of retrograde transport in the absence of concurrent anterograde transport. This property has made toxins and their nontoxic subunits useful tools for the study of retrograde transport (Majoul et al., 1996, 1998; Sandvig and van Deurs, 1996; Johannes et al., 1997; Llorente et al., 1998; Mallard et al., 1998). Some toxins of this class, such as PE and CT, have KDEL or KDEL-like signals and rely on the signal-mediated, COPI-dependent pathway for ER arrival from the Golgi (Majoul et al., 1998; Jackson et al., 1999). Others appear to reach the ER independent of these mechanisms. For example, the B-subunit of Shiga toxin arrives in the ER efficiently with or without a KDEL signal (Johannes et al., 1997). Consistent with this, inhibition of KDEL-mediated retrieval inhibits ER arrival and toxicity of PE, but SLT transport and toxicity is unaffected (Jackson et al., 1999), indicating SLT can reach the ER by a different mechanism. Extending this, Girod and coworkers have recently shown that inhibition of COPI function in vivo inhibits Golgi→ER retrograde transport of PE, but SLT and STB-fragment are unaffected (Girod, A., B. Storrie, J.C. Simpson, J.M. Lord, T. Nilsson, and R. Pepperkok, manuscript submitted for publication). Retrograde transport of a subset of toxin proteins thus has different functional requirements from the known signal-mediated, COPI-dependent pathway, strongly suggesting that they follow a fundamentally different transport route to the ER. The question remains whether they induce a new pathway, or usurp a pre-existing cellular pathway, and what cellular components might mediate such retrograde transport.

One cellular component that has been implicated in retrograde transport but has not been put into the context of the signal-mediated, COPI-dependent pathway for ER retrieval is the small GTPase Rab6. In general, Rab proteins cycle between GDP- and GTP-bound forms that correspond to their active and inactive states (Martinez and Goud, 1998). Rab proteins tend to be confined to specific membrane systems, and the current model of Rab function posits they act as molecular switches or timers to regulate transport between compartments (Novick and Zerial, 1997). By interacting with specific effectors, Rabs may in fact define the molecular identity of a compartment, making them excellent markers for correlating compartment function with compartment morphology and dynamics (Simons and Zerial, 1993). Rab6 is associated with the Golgi and TGN by immunoelectron and light microscopy (Goud et al., 1990; Antony et al., 1992). Consistent with this localization, Rab6 was shown to regulate transport between early and late Golgi compartments. Specifically, overexpression of GTP-bound forms of Rab6 inhibits an anterograde transport step within the Golgi, and induces a progressive, microtubule-dependent redistribution of Golgi resident proteins to the endoplasmic reticulum (Martinez et al., 1994, 1997). Since the GTP-bound forms of Rab proteins are thought to be the active species, and flux through the Golgi is likely a balance of anterograde and retrograde processes, a likely interpretation is that Rab6:GTP inhibits anterograde transport indirectly by stimulating retrograde transport at the level of the Golgi, or possibly between the Golgi and the ER (Martinez et al., 1997). In favor of the second possibility, Rab6 associates directly with a novel kinesin, Rabkinesin-6, capable of long range movement on microtubules (Echard et al., 1998) and translocation to the peripheral ER.

To provide a more detailed intracellular context for the molecular events which Rab6 regulates, we made fluorescent protein (FP) fusions to Rab6. Recently, observation of protein dynamics in live cells using fusions to the green fluorescent protein (GFP) has provided dramatic new insight into the function of the secretory pathway (Presley et al., 1997; Scales et al., 1997). Using live cell confocal laser scanning microscopy we observed the dynamics of FP-Rab6 in living cells. We find that the compartment defined by FP-Rab6 is highly dynamic, and FP-Rab6 trafficking elements exhibit properties of intracellular transport carriers. To relate FP-Rab6 dynamics to known components of the exocytic pathway, we used live cell double-labeling with different fluorescent proteins to directly compare two components in the same living cell (Ellenberg et al., 1998). The wild-type Shiga toxin B-fragment and FP-Rab6 traffic together during the time STB undergoes retrograde transport from the Golgi to the ER, but components of the COPI-dependent Golgi→ER pathway segregate away from FP-Rab6 and STB trafficking structures. Like STB ER arrival (Girod et al., 1999). FP-Rab6 trafficking is COPI independent. Overexpression of the Rab6:GDP (T27N) mutant of Rab6 reduces toxicity of Shiga holotoxin, indicating that native Rab6 regulates Golgi→ER transport. We propose that Rab6 regulates a novel, morphologically and mechanistically distinct cellular transport pathway from the Golgi to the ER.

Materials and Methods

Fluorescent Protein Fusion Constructs

YFP, GFP, and CFP indicate yellow, green, and cyan fluorescent proteins, respectively, and refer to GFP spectral variants based on the 10C (yellow), S65T (green), and W7 (cyan) mutants (Heim et al., 1994, 1995; Heim and Tsien, 1996). The parent vectors for all constructs were pEGFP-N1 (GenBank accession number U55762) or pEGFP-C3 (GenBank accession number U57607; Clontech Laboratories). Yellow variants of these vectors

were generated by subcloning an AgeI-BsrGI fragment from the vector pEYFP-C1 (Clontech Laboratories) into the vector backbone of pEGFP-N1 or -C3 digested with AgeI and BsrGI. Cyan variants of these vectors were generated by subcloning an AgeI-BsrGI fragment encoding ECFP from the vector pRSET-ECFP (Miyawaki et al., 1997; graciously provided by Roger Tsien) into the vector backbone of pEGFP-N1 or -C3 digested with AgeI and BsrGI. All inserts into these vectors that were generated by PCR were sequenced on both strands using flanking primers.

GFP-Rab6 comprises GFP fused to the NH_2 terminus of the corresponding full-length human Rab6 protein. A DNA fragment encoding the Rab6 wild-type protein (Martinez et al., 1994; *rab6* GenBank accession M28212) was generated by PCR to insert an in-frame BsrGI site at the 5′ end, and a stop codon followed by a NotI site at the 3′ end and inserted into pEGFP-N1 to generate pEGFP-Rab6wt. An alternate plasmid that varied slightly in the spacing between GFP and the Rab6 protein was constructed by inserting the *rab6* cDNA into the EcoRI-BamHI sites of pEGFP-C3 to generate pEGFP-Rab6wt′. No differences in trafficking or localization between the two constructs were observed. Stable cell lines (below) were generated with pEGFP-Rab6wt. Color variants were generated from pEGFP-Rab6wt′ (pEYFP-Rab6wt′ and pECFP-Rab6wt′).

KDELR-GFP comprises GFP fused to the COOH terminus of the full-length human KDEL-receptor (Erd2.1). A cDNA was generated that contained the *erd2.1* sequence (GenBank accession X55885) with an EcoRI site and Kozak consensus at the 5′ end, and a BamHI site replacing the *erd2.1* stop codon at the 3′ end. It was inserted into pEGFP-N1 to yield pKDELR-GFP and subcloned into pEYFP-N1 and pECFP-N1 to generate pKDELR-YFP and pKDELR-CFP.

GFP-Sec61β was kindly provided before publication and is described (Rolls et al., 1999). In brief, it is comprised of GFP fused to the NH_2 terminus of the full-length human Sec61β, with a short linker sequence between, constructed in a derivative of the vector pcDNA3.

Cells, Tissue Culture, and Generation of Stable Cell Lines

HeLa (ATCC No. CCL 185) and PtK_2 cells (ATCC CCL 56) were cultured in 5% fetal calf serum as described previously (White et al., 1998; Toomre et al., 1999). Stably transfected cell lines were generated by fluorescent cell sorting essentially as described (Le Bot et al., 1998; White et al., 1998). Lines were resorted as required to maintain the homogeneity of the population.

Antibodies, Immunofluorescence, and Immunoelectron Microscopy

The following antibodies were used: anti-Giantin mouse monoclonal (kind gift of H.P. Hauri, Biozentrum, Basel, Switzerland; Linstedt and Hauri, 1993; 1:200 for immunofluorescence); anti–β-tubulin mouse monoclonal (1:2,000 for blotting, 1:200 for IF; Boehringer-Mannheim); anti-Rabkinesin-6 rabbit polyclonal (Echard et al., 1998; 1:100 for IF); anti-Paxillin monoclonal (1:500 for IF; Transduction Laboratories); anti-β COP mouse monoclonal E5A3 (Duden et al., 1991; neat for IF); anti-β′ COP mouse monoclonal (Palmer et al., 1993; neat hybridoma supernatant for IF); anti-Erd2 (anti-KDLER; kindly provided by Joachim Füllekrug; Le Bot et al., 1998; Majoul et al., 1998; 1:100 for IF); anti-Rab6 rabbit polyclonal (Goud et al., 1990; 1:50 to 1:100 for IF); anti-GFP rabbit polyclonal (kind gift of Ken Sawin, Cell Cycle Laboratory, ICRF, London, UK; Shima et al., 1997; 1:50 and 1:100 for immuno-EM). Secondary antibodies were Cy3-conjugated donkey anti–rabbit and Cy3-conjugated donkey anti-mouse (each at 1:1,000 for IF; Dianova).

For indirect immunofluorescence, cells grown on glass coverslips were fixed 20 min in PBS + 3% paraformaldehyde (PFA) at room temperature or 2 min in neat methanol at −20°C, and processed using standard protocols described in Louvard et al. (1982). For immunofluorescence with anti-Rab6 antibody, the staining was performed as described in Martinez et al. (1994). Coverslips were mounted in Moviol (Hoechst), or viewed under live cell conditions (see below) at room temperature in PBS.

Immunoelectron microscopy was performed as described in Röttger et al. (1998), a modification of the protocol in Nilsson et al. (1993), using affinity-purified rabbit polyclonal anti-GFP antibody.

Transient Transfections and Microinjections

All transfections used a calcium phosphate protocol as described (Pääbo et al., 1986).

Experiments to determine the effect of transient overexpression of native Rab6 wild-type, T27N, Q72L proteins on GFP-Rab6 motility were performed two ways: expression constructs for the native protein (identical to the GFP-Rab6 vector except without the GFP) were (a) cotransfected with GFP-Rab6 at various molar ratios: 0.25, 0.5, 0.75, and 0.90 (native wild-type or mutant:GFP-Rab6) into untransfected HeLa or PtK_2 cells; or (b) cotransfected with a construct expressing soluble BFP as a live cell transfection marker into GFP-Rab6 HeLa or PtK_2 stable cell lines. The degree of cotransfection was monitored by immunofluorescence with anti-Rab6 antibody and by control experiments where the BFP expression construct was cotransfected with pEGFP-Rab6wt. Cotransfected cells were visualized 12, 18, 24, and 36 h after removal of the precipitate.

For live cell double-labeling experiments with fluorescent protein spectral variants, cells were transiently cotransfected with CFP and YFP-fusion protein expression constructs mixed in equal amounts by weight before transfection. Cotransfected cells expressing approximately equal levels of CFP and YFP-fusion proteins (based on relative fluorescent intensity) were imaged 18–36 h after removal of the transfection precipitate. FP-Rab6 localization and trafficking were not detectably affected by incubation at the different temperatures used for the STB internalization (see below).

Microinjection of anti-EAGE was performed as described (Pepperkok et al., 1998; Pepperkok et al., 1993).

Live Cell Confocal Microscopy, Two-Color Fluorescent Protein Double-labeling, and Image Processing

Live cell confocal microscopy was performed on the Compact Confocal Camera (CCC) as described previously (White et al., 1998). Cells were maintained on the microscope stage using an FCS2 system (Bioptechs) for perfusion experiments, or a slide chamber fitted for 15-mm round coverslips, together with an objective heater (Bioptechs). Cells were imaged in DME (HeLa) or MEM (PtK_2) that had been preequilibrated in a 5% CO_2 incubator. All images were taken with a 63× 1.4 NA Plan-Apochromat III DIC objective (Carl Zeiss). For multi-channel imaging, each fluorescent dye was imaged sequentially in either frame-interlace or line-interlace modes to eliminate cross-talk between the channels. EGFP fluorescence was excited with 488 nm argon-ion laser line and imaged using a NT80/20/543 beamsplitter and a 505-nm longpass emission filter. Cy3 fluorescence was excited with a 543-nm HeNe laser and imaged through a 560-nm longpass emission filter. CFP was excited with a 430-nm laser line (Directly Doubled Diode/D^3, Coherent) and imaged through a combination of 440–505-nm bandpass and 525-nm longpass emission filters. YFP was exited with the 514-nm laser line and imaged through a 525-nm longpass emission filter. Cross-talk in this configuration was quantitated; YFP signal in the CFP channel was below detectable limits. CFP in the YFP channel was 4% of the signal in the CFP channel, adjusted for illumination intensity.

All image processing was performed on a Macintosh computer using the public domain NIH Image program version 1.62 (developed at the US National Institutes of Health and available on the Internet at http://rsb.info.nih.gov/nih-image/). Eight-bit movies from two channels were overlaid to produce 16- or 24-bit color Quicktime movies in Adobe Premier. NIH Image macros used for data processing are available at http://www.embl-heidelberg.de/~jwhite/. Adobe Photoshop 5.02 and Illustrator 8.0 were used to prepare final figures for publication.

Additional image processing procedures and image correlation analysis to quantitate colocalization and motility are described in the online supplemental material.

STB Purification, Labeling, Uptake, and Temperature Shift Protocols

Recombinant wild-type Shiga toxin B-fragment was purified as described (Su et al., 1992; Johannes et al., 1997). The wild-type fragment contains no KDEL sequence or other known signals for ER retrieval and localization (Johannes et al., 1997). Purified STB was labeled with Cy3 according to manufacturer's instructions (Amersham Life Science, Inc.) as in previous studies (Mallard et al., 1998).

STB internalization experiments were performed as described (Johannes et al., 1997; Mallard et al., 1998). Imaging was initiated by flipping

the coverslip into a slide chamber at the imaging temperature (37 or 28°C, as indicated), focusing, and starting the preoptimized time-lapse program on the CCC. All STB experiments were performed with HeLa cells, since PtK_2 cells did not bind the labeled STB.

Rab6 T27N Overexpression and Toxicity Assays

HeLa cells were mock transfected or transfected with mutant Rab6 expression plasmids basically as described (Martinez et al., 1994). In brief, 10^5 HeLa cells were for 30 min infected with T7 polymerase expressing vaccinia virus (Fuerst et al., 1986) and then transfected with 3 μg of vector DNA using DOTAP (Boehringer). After 2 h, serum-free transfection medium was replaced by medium containing 10% fetal calf serum (Life Technology). Transfection efficiency as determined by immunofluorescence analysis was routinely above 80%. Functional assays were performed as described below in the continuous presence of 10 mM hydroxyl urea (Sigma Chemical Co.).

Purified Shiga toxin was added to the cells at the indicated concentrations. The cells were incubated for 100 min at 37°C, put on ice, and washed 2 times with leucine-free MEM medium (Life Technology). After addition of 1 μCi/ml of [^{3}H]leucine (151 Ci/mmol; Amersham) in ice-cold medium, the cells were transferred to 37°C for 20 min, washed and lysed in 0.1 M KOH on ice, and proteins were precipitated with TCA. Incorporation of radioactive leucine was determined by liquid scintillation counting after filtration on GF/C filters (Whatman).

Scatchard analysis was done as described (Johannes et al., 1997) using B-fragment iodinated with IodoBeads (Pierce) to a specific activity of 5,000 cpm/ng.

Online Supplemental Material

Movies corresponding to Figs. 2–8 are available online along with instructions for viewing them. Additional Materials and Methods describe how image correlation analysis was used to quantitate colocalization and motility. Available at http://www.jcb.org/cgi/content/full/147/4/743/DC1.

Results

Characterization of GFP-Rab6

To observe the dynamics of Rab6 in live cells we fused fluorescent proteins (cyan, green, or yellow) to the NH_2 terminus of wild-type Rab6 to generate FP-Rab6. Fig. 1 a shows the overall topology of the fusion protein and putative orientation in a membrane bound state. We used FACS® to generate HeLa and PtK_2 cell lines stably expressing GFP-Rab6. In these cells, GFP-Rab6 associated with compact structures next to the nucleus, consistent with localization to the Golgi. Diffuse fluorescence was observed in brighter cells, and likely represented a cytosolic pool of GFP-Rab6. Western blotting of whole cell extract showed GFP-Rab6 was mildly overexpressed in the stable HeLa cell line (Fig. 1 b). At the ultrastructural level, cryoimmunoelectron microscopy using an antibody against GFP showed labeling of GFP-Rab6 over Golgi stacks and associated tubulovesicular elements, with no significant labeling over other structures (Fig. 1 c). CLSM and immunofluorescence showed that the GFP-Rab6 fluorescence adjacent to the nucleus colocalized with the Golgi protein Giantin (Fig. 1 d). GFP-Rab6 was also present in structures that were devoid of Giantin, in punctate peripheral elements, and at distinct sites in the corners of the cell that were near sites containing Paxillin, a focal adhesion component (Fig. 1 e). The punctate GFP-Rab6 elements were superficially similar in appearance to endosomes, but they did not colocalize with a number of endosomal markers. In fixed cells, transferrin receptor failed to colocalize with GFP-Rab6 peripheral elements (data not shown). In live cells, rhodamine-transferrin internalized for short or long periods did not coincide with FP-Rab6, nor did a fluorescent protein fusion to Rab5, a marker of early endosomes, nor did fluorescently labeled Shiga toxin B-fragment blocked in endosomes at 19.5°C (data not shown). Visualization of the lysosome-specific vital dye LysoTracker in live FP-Rab6 cells showed different dynamics and no colocalization with FP-Rab6 trafficking structures (data not shown).

To determine if stable GFP-Rab6 expression altered the endogenous Rab6 compartment, we immunolocalized the Rab6 effector Rabkinesin-6 in GFP-Rab6 HeLa cells (Fig. 1 f). Since anti-Rab6 antibodies recognize GFP-Rab6 (Fig. 1 b), precluding comparison of native and GFP-Rab6, it was not meaningful to localize native Rab6 in GFP-Rab6 cells. Overall Rabkinesin-6 distribution was consistent with its reported localization in untransfected cells (Echard et al., 1998). GFP-Rab6 structures at the very periphery did not colocalize with Rabkinesin-6 (arrows).

FP-Rab6 localized to the Golgi complex, was consistent with the localization of endogenous Rab6, and did not obviously affect the distribution of a Rab6 effector. These results suggest that the intracellular compartment defined by FP-Rab6 in living cells was relevant to the compartment defined by native Rab6.

FP-Rab6 Dynamics in Live Cells

To observe the dynamics of the intracellular compartment defined by FP-Rab6 in living cells, we observed GFP-Rab6 HeLa and PtK_2 stable cell lines using time-lapse live cell microscopy. Standard imaging conditions used confocal laser scanning microscopy (CLSM) to collect single confocal slices every 1–10 s for periods of 5 to >60 min. The GFP-Rab6 compartment was highly dynamic. It consisted of a stable Golgi region, motile peripheral trafficking elements, a diffuse network with a nebulous appearance, and distinctive accumulations in distal corner regions (Fig. 2 a, and supplemental movies at http://www.jcb.org/cgi/content/full/147/4/743/DC1). Discrete globular and long (>2 μm) tubular structures exited the Golgi and translocated outward along curvilinear paths to the cell periphery. Trafficking elements translocated at ~0.6–1 μm/s. The primary flux of GFP-Rab6 trafficking was away from the Golgi toward the cell periphery, but some elements translocated from the periphery to the Golgi and entered, some left and reentered, and tubules occasionally extended and then retracted. A brightest-point projection through the movie (Fig. 2 b, and supplemental movies at http://www.jcb.org/cgi/content/full/147/4/743/DC1) shows the tracks followed by trafficking structures, and indicates the high probability of elements trafficking through the corner regions. The corner regions were highly dynamic; we observed trafficking elements enter and coalesce there, exit and traffic between sites, and exit and disperse into the diffuse network. Dispersal was not due to trafficking structures simply moving out of the plane of focus, since we observed fluorescence disperse laterally within the focal plane and this dispersion was clearly distinguishable from trafficking structures which did move in and out of focus. The diffuse network had dis-

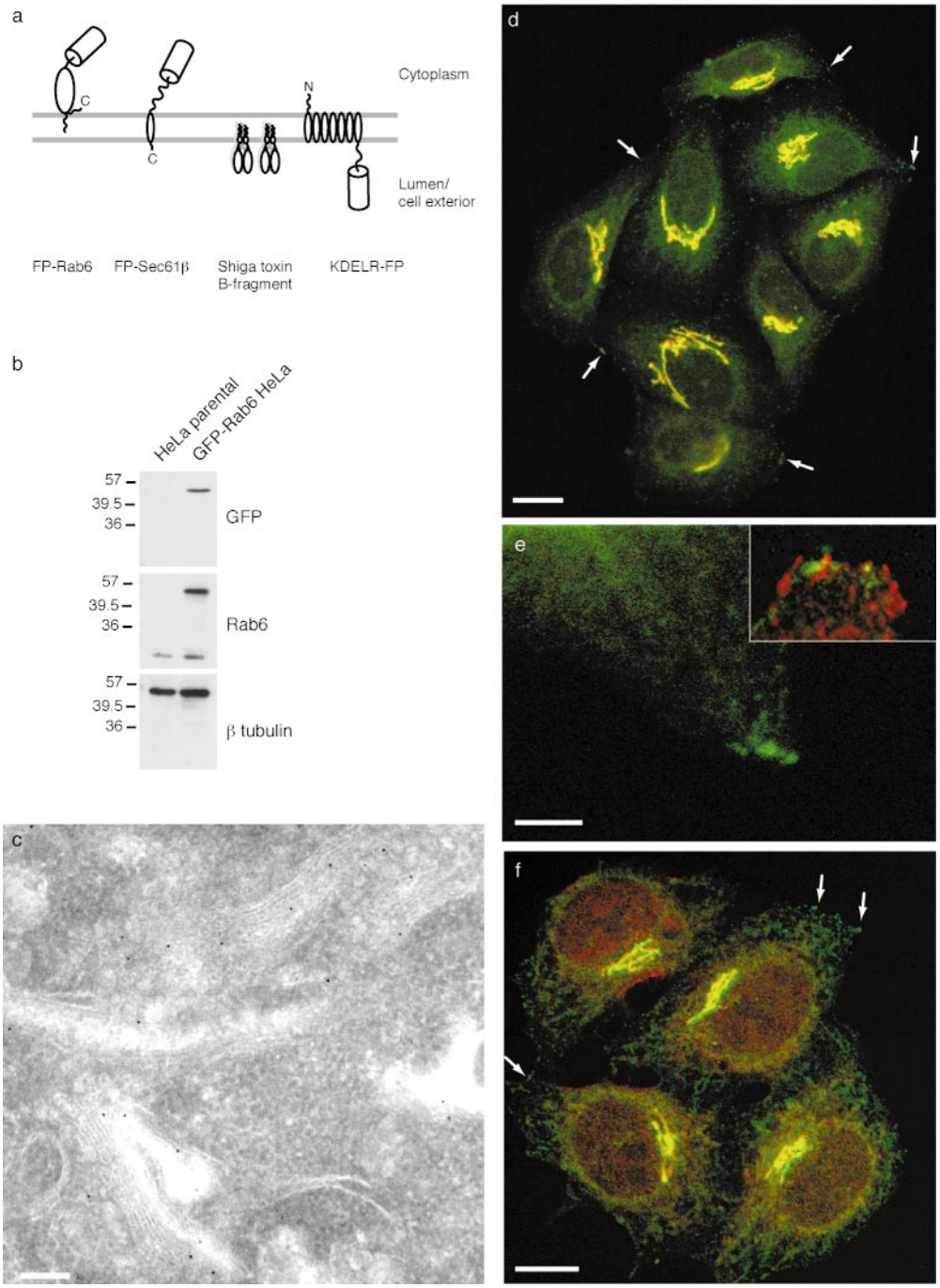

Figure 1. Characterization of GFP-Rab6. (a) Fluorescent markers used in this study. (b) GFP-Rab6 is moderately overexpressed in stable cell lines. Whole cell extract from either stably transfected GFP-Rab6 HeLa cells or the untransfected parental cell line were blotted and probed with antibodies against GFP or native Rab6. Three sets of lanes were cut from the same gel. β-tubulin was probed as a loading control. (c) GFP-Rab6 localizes to Golgi stacks and associated tubular-vesicular profiles. Cryo-immunoelectron microscopy of GFP-Rab6 HeLa cells stained with anti-GFP antibody and detected with 10 nm gold. (d) Stably expressed GFP-Rab6 localizes to the Golgi and to peripheral elements. GFP-Rab6 (green) and the Golgi marker Giantin (red) in fixed cells. GFP-Rab6 fluorescence is from GFP; Giantin was visualized by immunofluorescence. Arrows point to representative GFP-Rab6 peripheral elements. The image is a single confocal section. (e) Peripheral GFP-Rab6 elements (green) and corner regions do not contain detectable Giantin (red, not visible), but are close to focal adhesions, revealed by Paxillin staining (inset, red). Cells fixed and stained as in D; single confocal section. (f) GFP-Rab6 expression does not alter the intracellular distribution of a Rab6 effector. Rabkinesin-6 (red) in fixed GFP-Rab6 cells. Brightest-point projection through 9 confocal sections taken every 0.7 μm. Arrows point to representative GFP-Rab6 elements that do not colocalize with Rabkinesin-6. Bars: (c) 250 nm; (d–f) 10 μm.

tinct dynamics and structure, and was closely associated with the trafficking elements and corner regions.

We observed slight differences in GFP-Rab6 trafficking within a population of cells. Some cells were more active, as judged by the number of globular and tubular GFP-Rab6 trafficking elements and their frequency of translocation. Not all cells in a population showed accumulation in peripheral corner regions, but we always observed significant trafficking to these areas. Occasionally, the tubular structures extending from the Golgi were quite dramatic, extending all the way to a peripheral endpoint without detaching (see Fig. 5 a). We observed no substantial differences between trafficking in PtK_2 and HeLa cells, although tubulation was slightly less apparent in PtK_2

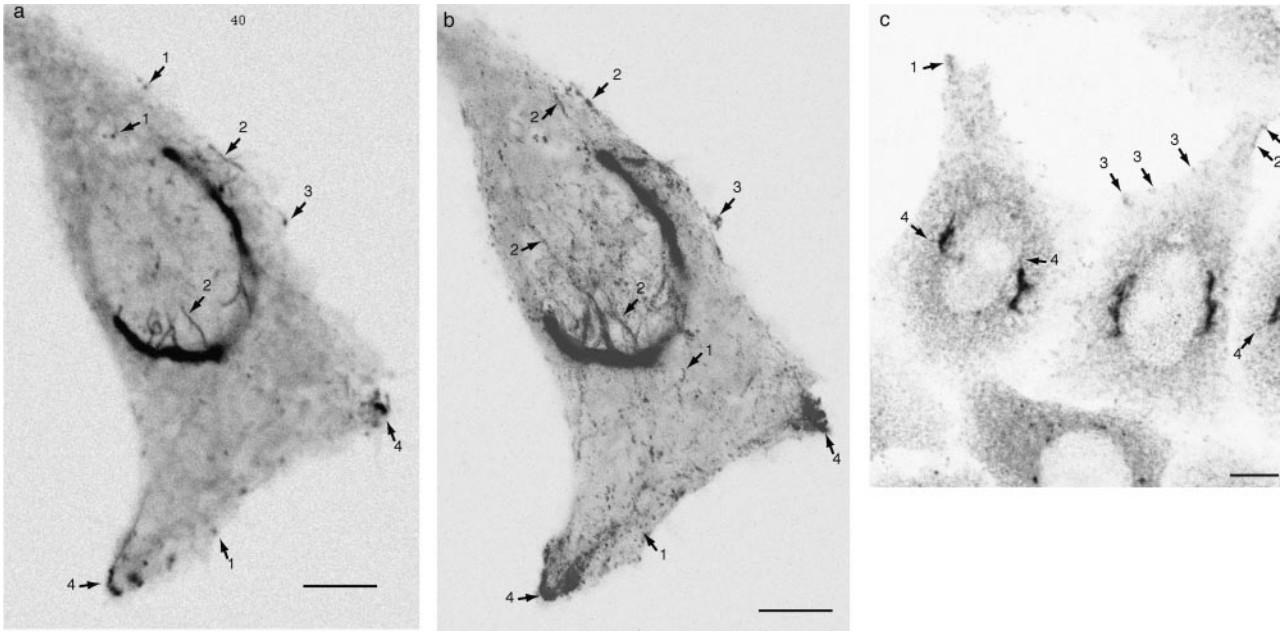

Figure 2. GFP-Rab6 trafficking in live cells is highly dynamic and reveals features of endogenous Rab6. See also the Fig. 2 movies at http://www.jcb.org/cgi/content/full/147/4/743/DC1. (a) Representative dynamic GFP-Rab6 elements. GFP-Rab6 stably expressed in a HeLa cell visualized over time at 37°C on a confocal laser-scanning microscope. Shown is a single confocal frame from a movie of 180 images taken at 1 frame/s. Representative globular (1) and tubular (2) trafficking elements are indicated with arrows. The diffuse network is visible as an irregular pattern in the cytosolic signal (also visible in b). Distinctive GFP-Rab6 edge (3) and corner (4) regions are indicated. The plane of focus is below the nucleus. Images are inverted. (b) GFP-Rab6 dynamics over time. Brightest-point projection of all 180 images of the movie in a. Movement appears as a series of dots for globular elements (1), and snake-like streaks for tubular elements (2). The high flux through the corner regions is indicated in the projection by an apparent accumulation in these regions (4, compare a with b). The line of dots between the peripheral corner points indicates trafficking between them. Blotchiness in the cytoplasmic regions indicates the underlying diffuse network. (c) Native Rab6 localizes to structures similar to those defined by GFP-Rab6. Immunofluorescence of endogenous Rab6 in untransfected HeLa cells shows the same features noted in a and b. Arrows point to corner regions (1), tubular elements (2), globular elements (3), and tubules extending from the Golgi (4). Bars, 5 μm.

cells. Live cell double-labeling experiments with a Golgi marker, T2-CFP (White et al., 1998) and YFP-Rab6 showed FP-Rab6 trafficking did not reflect the dynamics of the Golgi itself, and behavior was specific to the Rab6 fusion, since FP-Rab6 trafficking did not resemble trafficking of an analogous fusion to the Golgi-associated Rab8 protein (data not shown).

The level of GFP-Rab6 did not observably affect trafficking, indicating GFP-Rab6 trafficking structures were not induced by GFP-Rab6 expression. High expression levels of GFP-Rab6, indicated by comparing variations in fluorescence intensity within a population, resulted in higher levels of cytosolic fluorescence rather than increased trafficking activity (not shown). Transient overexpression of native Rab6 wild-type or GTP-mutant (Q72L) in GFP-Rab6 cells using a CMV promoter vector also had no noticeable effect on trafficking (see Materials and Methods). Overexpression of native Rab6 wild-type or Q72L using the T7 vaccinia system dispersed GFP-Rab6 into diffuse cytosolic fluorescence (data not shown).

To establish whether GFP-Rab6 trafficking elements were relevant to the role of native Rab6, we performed immunofluorescence with anti-Rab6 antibody in untransfected HeLa cells. Careful observation revealed that native Rab6 shares many features with GFP-Rab6. Fig. 2 c shows fixed, untransfected HeLa cells stained with anti-Rab6 polyclonal antibody and examined by CLSM. Peripheral corner regions (1), peripheral tubular and globular elements (2 and 3), and tubules extending from the Golgi (4) are all apparent. These observations suggest that GFP-Rab6 reveals relevant features of the membrane system defined by native Rab6, and further indicate that GFP-Rab6 expression does not induce abnormal trafficking structures.

Since native Rab6 associates with a microtubule-dependent kinesin, Rabkinesin-6, we determined whether GFP-Rab6 trafficking elements translocated along microtubules. To establish a requirement for microtubules, we treated GFP-Rab6 HeLa or PtK_2 cells with nocodazole, which prevents dynamic microtubules from repolymerizing, and observed the effects directly in live cells. During the first 10 min of nocodazole exposure, the flux of GFP-Rab6 trafficking concentrated along a few linear tracks, which would be consistent with a flux directed along remaining stable microtubules. After this period, long-range GFP-Rab6 trafficking ceased, showing microtubules were required for long-range GFP-Rab6 translocation (not shown). To directly show FP-Rab6 trafficking along microtubules, we performed live cell double-labeling experiments with CFP- or YFP-tubulin and YFP- or CFP-Rab6. FP-Rab6 trafficking elements translocated along fluorescent microtubules; corner regions and peripheral sites cor-

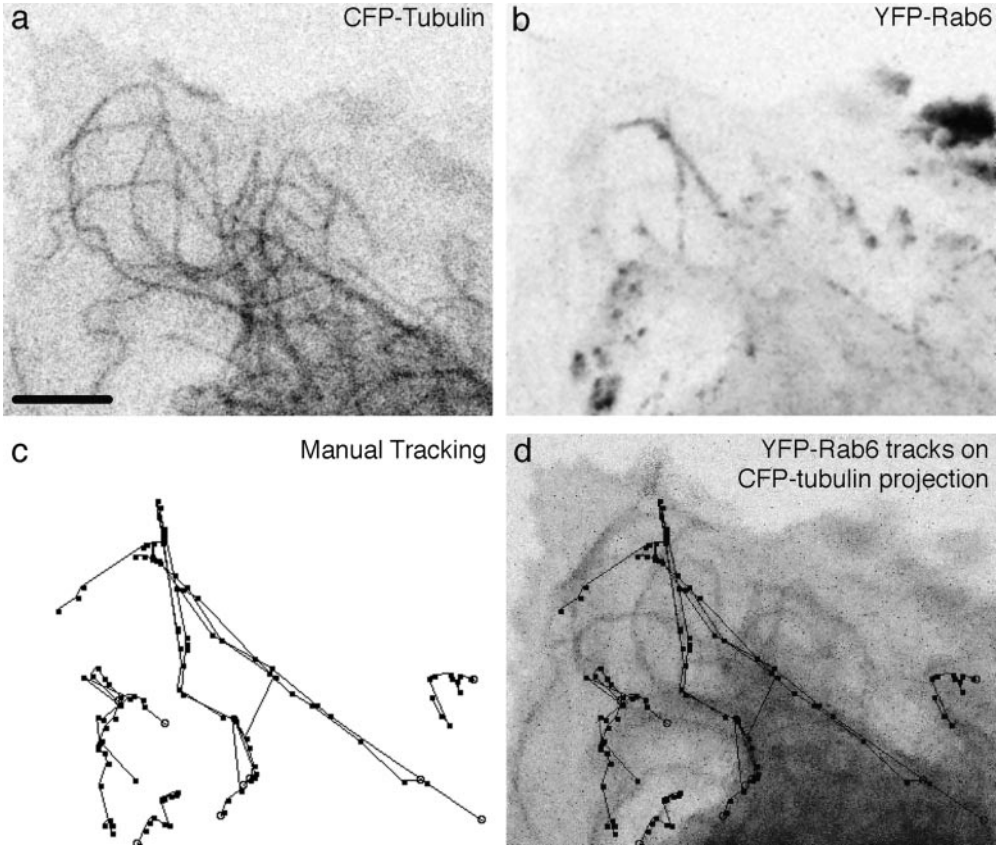

Figure 3. FP-Rab6 trafficking elements translocate along microtubules. See the Fig. 3 movies and additional movies online at http://www.jcb.org/cgi/content/full/147/4/743/DC1. CFP-Rab6 and YFP-tubulin were transiently cotransfected and observed together in a live PtK_2 cell. The peripheral edge of the cell is shown. (a) YFP-tubulin at the peripheral edge of a cell. Single confocal slice at the start of the movie. (b) CFP-Rab6 over time. Projection of 25 confocal images taken every 8.8 s. (c) Manual tracking of selected CFP-Rab6 elements over time. Ten of the most visually prominent moving elements were tracked over the course of the movie. Stable elements are near the tips of microtubules, but do not move significantly and so were not tracked. (d) CFP-Rab6 tracks follow microtubules over time. Tracks from c overlaid on a projection of 25 YFP-tubulin images. Bar, 5 μm.

responded to the ends of labeled microtubules (Fig. 3, and supplemental movies at http://www.jcb.org/cgi/content/full/147/4/743/DC1). Together these two results show GFP-Rab6 elements traffic along microtubules.

To ascertain whether the trafficking that we detected at the acquisition frequency of the laser-scanning microscope (1–10 s/frame) was a complete representation of GFP-Rab6 trafficking, we imaged GFP-Rab6 in live cells with conventional fluorescence and fast CCD detection to acquire images every 100–500 ms. GFP-Rab6 trafficking observed at rapid acquisition rates was substantially the same, considering the lower spatial resolution of this approach and the out-of-focus haze that obscured the objects in focus (see Fig. 2 supplemental movie at http://www.jcb.org/cgi/content/full/147/4/743/DC1). Together with direct observation by eye, the fast CCD acquisition makes it highly unlikely that we have missed detecting significant fast-moving GFP-Rab6 structures. Thus, our movies are an accurate representation of GFP-Rab6 trafficking.

Wild-type Shiga Toxin B-Fragment, a Retrograde Cargo, Traffics in GFP-Rab6 Structures

Since earlier studies provided evidence that Rab6 plays a role in retrograde transport, and FP-Rab6 trafficking structures appeared to be transport carriers translocating from the Golgi to the cell periphery, we determined whether they contained retrograde cargo. As a well characterized retrograde cargo, we used the wild-type B-fragment of Shiga toxin (STB; Fig. 1 a; Johannes and Goud, 1998). STB retrograde transport can be synchronized by binding the purified fragment to the cell surface at 4°C and initiating transport by shifting cells to 37°C (Johannes et al., 1997; Johannes and Goud, 1998; Mallard et al., 1998). We examined the retrograde transport of STB fluorescently labeled with Cy3 in live GFP-Rab6 HeLa cells. The overall pattern of STB transport was consistent with that previously described in untransfected HeLa cells (Johannes et al., 1997; Mallard et al., 1998). STB trafficking structures coincided with GFP-Rab6 trafficking during the time when STB undergoes transport from the Golgi to the ER (Fig. 4, a and b, and supplemental movies at http://www.jcb.org/cgi/content/full/147/4/743/DC1). Coincidence was first apparent at a time after STB had started to accumulate in the Golgi, 20–40 min after the shift to 37°C, and was most apparent until 60–90 min at 37°C. Tubular and globular structures labeled by both STB and GFP-Rab6 left the Golgi and traveled outward to peripheral sites. STB accumulated together with GFP-Rab6 in corner regions and seemed also to disperse outwards with GFP-Rab6 from these endpoints (Fig. 4). STB in corner regions became brighter, persisted for 60–90 min of internalization, and then gradually disappeared as ER fluorescence increased (compare Fig. 4, a with c). STB and GFP-Rab6 were not found in the same element at concentrations that gave comparable fluorescence intensities, making conventional colocalization difficult. Movies circumvented this problem

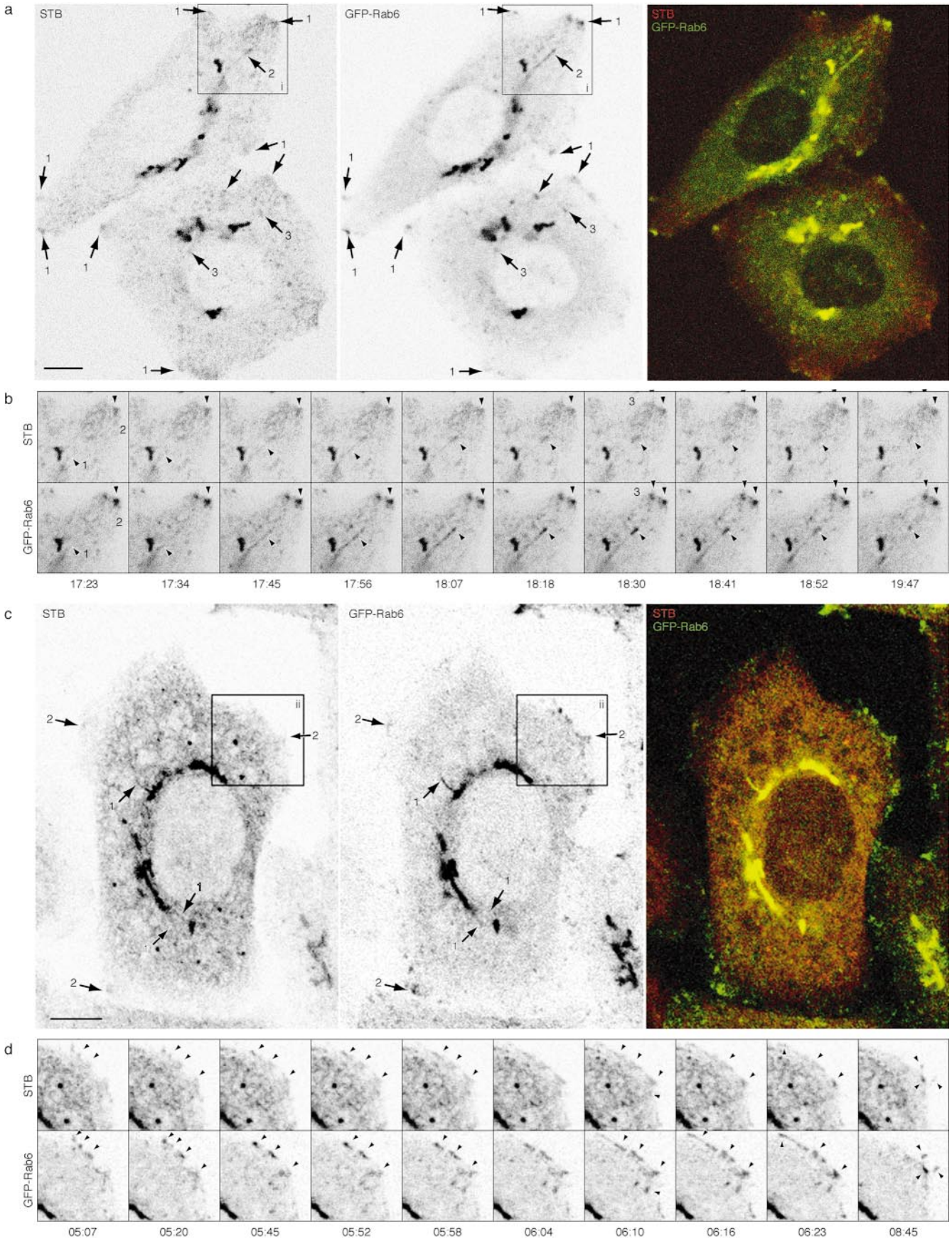
a
STB
GFP-Rab6
STB
GFP-Rab6
b
STB
GFP-Rab6
17:23
17:34
17:45
17:56
18:07
18:18
18:30
18:41
18:52
19:47
c
STB
GFP-Rab6
STB
GFP-Rab6
d
STB
GFP-Rab6
05:07
05:20
05:45
05:52
05:58
06:04
06:10
06:16
06:23
08:45

Figure 4.

by showing structures labeled by both proteins moving in the same manner over time.

To further compare STB and GFP-Rab6 trafficking we varied the temperature shift protocols. To compare STB endosome→Golgi transport with GFP-Rab6, STB was blocked in early endosomes at 19.5°C and then cells were shifted to 37°C to initiate transport (Mallard et al., 1998). At 19.5°C or directly after the shift, STB in early endosomes did not coincide with GFP-Rab6. Only after STB coalesced from early endosomes and began to accumulate in the Golgi and in peripheral corner regions did we observe coincidence of STB and GFP-Rab6 trafficking structures. To extend initial exit from the Golgi apparatus over a longer period of time, we bound STB at 4°C, pulsed it into the Golgi at 37°C for 15–25 min, and then shifted to 28–30°C (Fig. 4 a, and supplemental movies at http://www.jcb.org/cgi/content/full/147/4/743/DC1). Coincidence of GFP-Rab6 and STB trafficking was best under these conditions, with fewer extraneous structures that did not contain both proteins. These results are consistent with the hypothesis that GFP-Rab6 TCs are used by STB during the initial phase of transport from the Golgi to the ER.

STB trafficking structures also coincided with GFP-Rab6 trafficking at later times of STB internalization (Fig. 4, c and d). Coincident trafficking after 5 h of internalization was more difficult to discern because the high level of STB fluorescence in the ER obscured visualization of discrete trafficking structures, and not all GFP-Rab6 trafficking structures contained visible levels of STB. However, coincident trafficking was apparent in regions at the edge of the cell, where STB ER fluorescence was less intense (Fig. 4 d). Since at this time STB cycles between the ER and the Golgi (Johannes et al., 1997), this result is consistent with the idea that STB traffics extensively in GFP-Rab6 elements during the initial pulse of STB transport from the Golgi to the ER, and then continues to traffic in GFP-Rab6-positive structures during the retrograde stage of Golgi↔ER cycling.

To verify that FP-Rab6 trafficking structures specifically contained retrograde cargo, we observed a number of different anterograde cargo markers in live cell double-labeling experiments. In no case did we observe coincidence of these markers with peripheral FP-Rab6 trafficking elements (not shown). To verify that stable expression of FP-Rab6 did not induce STB trafficking structures, we observed STB transport live in untransfected HeLa cells using the same temperature shifts under the same imaging conditions. STB trafficking appeared the same as in the GFP-Rab6 stable cell line (not shown). Since STB and GFP-Rab6 trafficking structures were observed independently, it is unlikely that they are induced both by STB and by GFP-Rab6 expression. Rather, the coincident trafficking of the two proteins is consistent with a preexisting pathway.

FP-Rab6 Trafficking Is Distinct from Early-Golgi to ER Recycling

Since our results suggested GFP-Rab6 trafficking structures were retrograde transport carriers along a pathway from the Golgi to the ER, we determined whether they coincided with the Golgi→ER pathway used for the retrieval of ER residents and for the cycling of the KDELR and p24 proteins. As a marker for this pathway, we used a fluorescent protein fusion to the KDELR, KDELR-FP (Fig. 1 a). In stably transfected HeLa and PtK_2 cells, KDELR-FP distributed between a compact juxtanuclear region and the network of the ER, indicating that it localized properly (see supplemental movies at http://www.jcb.org/cgi/content/full/147/4/743/DC1). KDELR-FP showed characteristics of native KDELR; it accumulated in peripheral punctate structures upon incubation at 15°C and after treatment with BFA. Fluorescence loss in photobleaching (FLIP) experiments showed that the Golgi can be depleted of fluorescence by repeatedly photobleaching a region of the ER, indicating KDELR-FP exchanged from the Golgi to the ER (not shown). KDELR-FP thus reveals features of early Golgi↔ER cycling in live cells.

KDELR-GFP trafficking in live cells differed markedly from GFP-Rab6 trafficking (see supplemental movies for Fig. 6 at http://www.jcb.org/cgi/content/full/147/4/743/DC1). Tubulation was much less extensive, and globular elements translocated over shorter distances in a saltatory fashion, switching direction often. KDELR-GFP did not accumulate in corner regions, unlike both GFP-Rab6 and STB (Fig. 5 a, and supplemental movies at http://www.jcb.org/cgi/content/full/147/4/743/DC1). Unlike KDELR-GFP, GFP-Rab6 did not accumulate in peripheral punctate structures upon prolonged (2–4 h) incubation at 15°C (not shown). To test whether these

Figure 4. Wild-type Shiga toxin B-fragment traffics in GFP-Rab6 structures during Golgi→ER retrograde transport. See also the Fig. 4 movies at http://www.jcb.org/cgi/content/full/147/4/743/DC1. (a) STB traffics in GFP-Rab6 elements during initial Golgi→ER retrograde transport. Representative frame from a movie of 220 confocal images. Cy3-labeled STB was bound to GFP-Rab6 HeLa cells at 4°C and internalized at 37°C for 20 min to accumulate the fragment in the Golgi, then shifted to 28°C to prolong Golgi exit. Other temperature shift protocols were performed as described in Results with similar outcome. Arrows point to STB and GFP-Rab6 together in corner regions (1), in a tubule extending from the Golgi (2) and in globular trafficking elements (3). Images are inverted. (b) The dynamics of GFP-Rab6 and STB from region *i* in a. A tubule (1) containing both GFP-Rab6 and STB extends from the Golgi, detaches, and translocates to a peripheral corner region (2). STB and GFP-Rab6 accumulate together in peripheral corner regions and exhibit the same fluctuations in intensity (3). The time indicated is min:s since the beginning of imaging. Scale same as a. (c) STB continues to traffic in GFP-Rab6 structures during later times of STB internalization. Shown is a single frame from a movie of 250 confocal images initiated after 5 h of STB internalization at 37°C. Arrows point to STB and GFP-Rab6 in tubules extending from the Golgi (1), and in peripheral corner regions (2). (d) The dynamics of GFP-Rab6 and STB from region ii in c. Arrowheads point to structures where STB and GFP-Rab6 show the same dynamics. Time indicated is min:s after imaging was initiated at 5 h of STB transport. Several globular elements move toward the upper left and extend as a tubule at 6:04 and travel away at 6:23. By 8:45, other trafficking elements have entered the peripheral site and condensed there, extending out into projections from the cell. Bars: (a and b) 5 μm; (c and d) 10 μm.

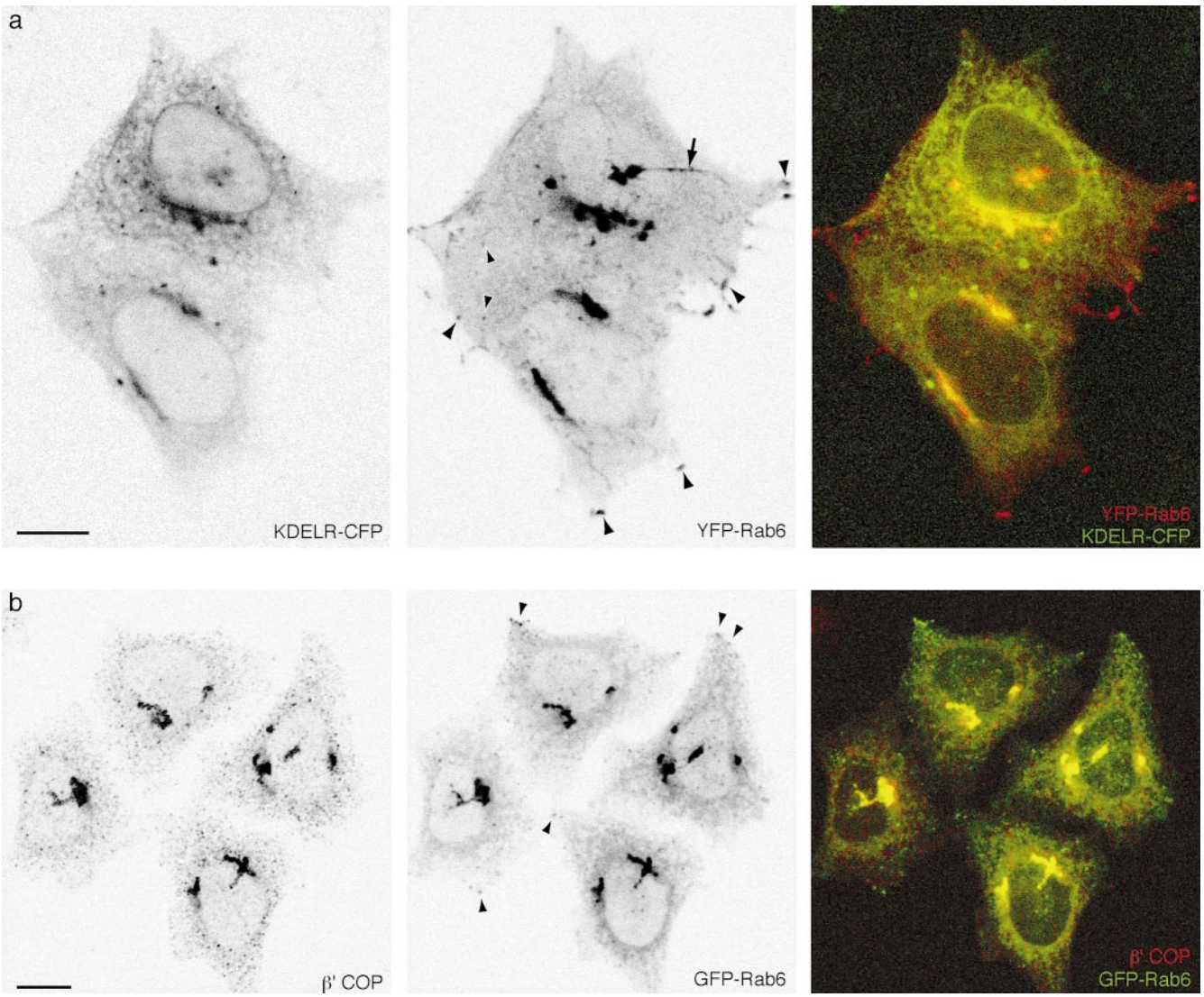

Figure 5. FP-Rab6 trafficking is distinct from Golgi→ER transport defined by KDELR-FP and COPI-coated peripheral structures. See also the Fig. 5 movies at http://www.jcb.org/cgi/content/full/147/4/743/DC1. (a) KDELR-CFP and YFP-Rab6 traffic in separate peripheral structures. KDELR-CFP and YFP-Rab6 were transiently cotransfected and observed together in a live cell. Shown is a single confocal slice; in the color overlay YFP-Rab6 is red and KDELR-CFP is green. An arrow points to a long YFP-Rab6 tubular element that extends to the cell periphery, it is devoid of detectable KDELR-CFP. Arrowheads point to representative globular YFP-Rab6 trafficking elements and corner regions that do not contain KDELR-CFP. The online movie shows a different cell (YFP-Rab6 in red and KDELR-CFP in green). (b) Peripheral GFP-Rab6 elements are separate from peripheral COPI-coated structures. GFP-Rab6 cells were fixed in PFA and stained for components of the COPI coatomer complex. Shown is a single confocal slice through GFP-Rab6 cells stained for β′-COP. Arrowheads show where GFP-Rab6 peripheral elements are separate from punctate structures positive for β′-COP. Bars, 10 μm.

differences represented a separation of peripheral trafficking elements, we performed live cell double-labeling experiments with KDELR-CFP and YFP-Rab6. In transiently cotransfected cells, KDELR-CFP and YFP-Rab6 peripheral trafficking elements did not coincide, and exhibited different dynamics in the same living cell (Fig. 5 a, and supplemental movies at http://www.jcb.org/cgi/content/full/147/4/743/DC1). Consistent with these results in live cells, immunofluorescence in fixed cells showed that endogenous KDELR peripheral elements did not overlap with GFP-Rab6 in the stably transfected cell line (not shown). These results suggest that FP-Rab6 trafficking is distinct from the KDELR-FP trafficking, and thus morphologically separate from the transport pathways used by the endogenous KDELR and KDELR-FP.

To further establish these differences, we compared the distribution of two different COPI coatomer subunits, β and β′, to peripheral GFP-Rab6 trafficking structures in the stably transfected HeLa cells. Immunofluorescence with antibodies against either β- or β′-COP showed that peripheral COPI structures were separate from peripheral GFP-Rab6 elements, and indeed seemed to exclude one another (Fig. 5 b). This result indicates that GFP-Rab6 trafficking elements are not COPI-coated.

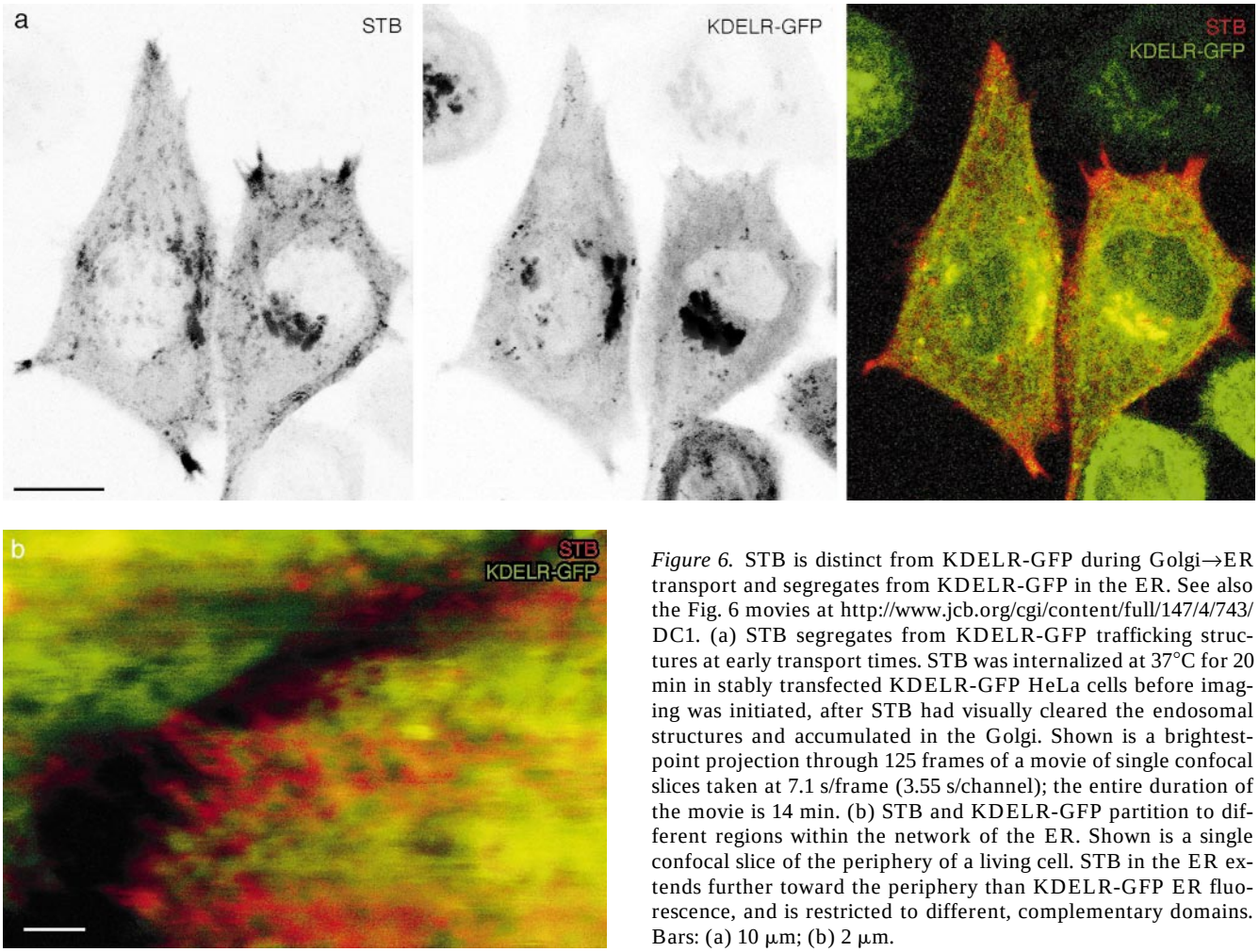

Figure 6. STB is distinct from KDELR-GFP during Golgi→ER transport and segregates from KDELR-GFP in the ER. See also the Fig. 6 movies at http://www.jcb.org/cgi/content/full/147/4/743/DC1. (a) STB segregates from KDELR-GFP trafficking structures at early transport times. STB was internalized at 37°C for 20 min in stably transfected KDELR-GFP HeLa cells before imaging was initiated, after STB had visually cleared the endosomal structures and accumulated in the Golgi. Shown is a brightest-point projection through 125 frames of a movie of single confocal slices taken at 7.1 s/frame (3.55 s/channel); the entire duration of the movie is 14 min. (b) STB and KDELR-GFP partition to different regions within the network of the ER. Shown is a single confocal slice of the periphery of a living cell. STB in the ER extends further toward the periphery than KDELR-GFP ER fluorescence, and is restricted to different, complementary domains. Bars: (a) 10 μm; (b) 2 μm.

Shiga Toxin B-Fragment Retrograde Transport Is Distinct from KDELR-GFP Trafficking

FP-Rab6 trafficking structures accumulated wild-type Shiga toxin B-fragment, but excluded KDELR and KDELR-FP. To determine whether STB trafficked in KDELR-GFP-positive as well as in GFP-Rab6-positive structures during transport to the ER, we observed STB transport in live KDELR-GFP HeLa cells (Fig. 6). At all times of transport, STB and KDELR-GFP tended to segregate from one another outside of the Golgi. At early times (15–120 min at 37°C), we observed little or no coincidence of STB and KDELR-GFP peripheral trafficking structures, and KDELR-GFP did not coincide with STB in corner regions (Fig. 6 a, see supplemental movies at http://www.jcb.org/cgi/content/full/147/4/743/DC1). At later times (2–5 h at 37°C), we observed partial coincidence of STB and KDELR-GFP globular trafficking structures, especially in cells that had internalized high levels of STB, but never coaccumulation in distinctive corner regions. After 5 h of internalization, after STB was readily visible in the ER network, STB partitioned to subdomains of the ER network that were depleted for KDELR-GFP fluorescence (Fig. 6 b); STB in the ER extended further to the cell periphery. These results are consistent with the observation that FP-Rab6 trafficking structures coincide with STB but not KDELR-FP, and provide morphological evidence that the bulk of STB is not transported to the ER via the pathway defined by KDELR-GFP. The partial coincidence may represent a minor proportion of STB that is transported via this pathway at later times, or it may represent mis-sorting into this pathway at high levels of STB.

Trafficking of KDELR-GFP, but Not GFP-Rab6, Depends on COPI

To determine whether the dynamic morphological differences we observed between FP-Rab6 and KDELR-FP represented functional differences between the two pathways, we inhibited COPI function in KDELR-GFP or GFP-Rab6 HeLa cells and observed the effect on trafficking. We microinjected anti-EAGE antibody, a potent inhibitor of COPI function in vivo (Pepperkok et al., 1993, 1998), and compared the dynamics of injected cells to uninjected cells in the same microscope field. In injected cells, the overall motility of KDELR-GFP was inhibited to 60% of an uninjected cell in the same movie, but GFP-Rab6 motility was not significantly inhibited (Fig. 7, see supplemental movies at http://www.jcb.org/cgi/content/full/147/4/743/DC1). These results indicate a functional

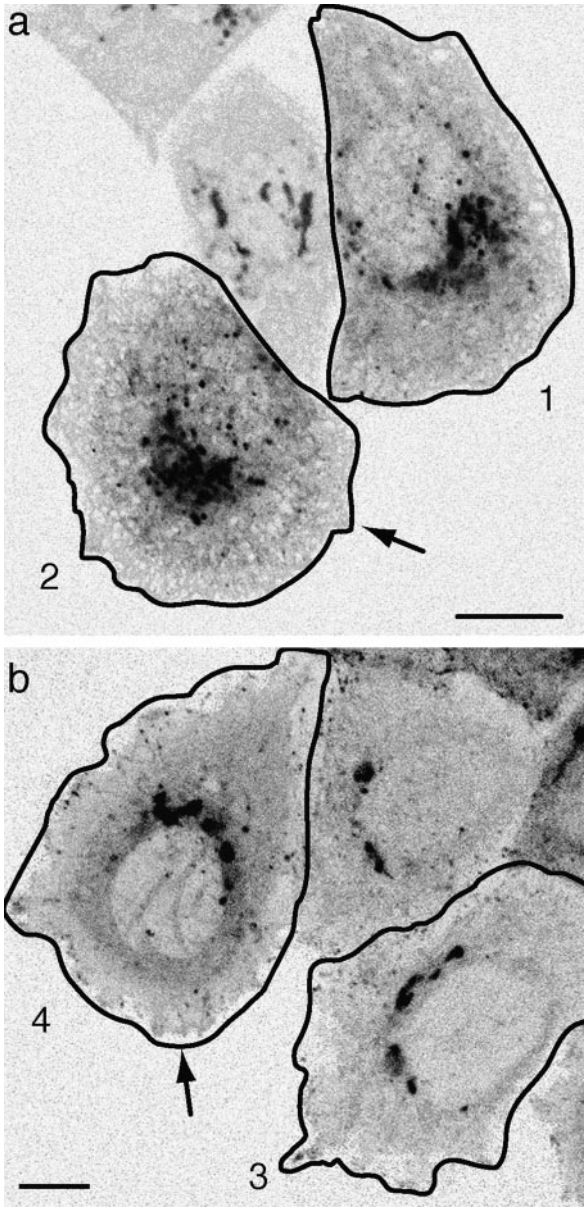

Figure 7. GFP-Rab6 trafficking does not depend on COPI function. See also the Fig. 7 movies and the Additional Experimental Procedures online at http://www.jcb.org/cgi/content/full/147/4/743/DC1. (a) Microinjection of anti-EAGE inhibits KDELR-GFP dynamics. Image from a movie of KDELR-GFP HeLa cells, injected (arrow) and uninjected. Imaging was initiated ~30 min after injection. A single frame was taken every 4 s for 26 min (395 frames). The focus is at the level of the ER; a cell adjacent to the injected cell has been pushed upwards by cell–cell contact. The regions used for correlation analysis to quantitate relative motion are outlined. (b) Microinjection of anti-EAGE does not inhibit GFP-Rab6 dynamics. Image from a movie of one injected (arrow) and two uninjected GFP-Rab6 HeLa cells. Imaging was initiated ~30 min after injection. A single frame was taken every 5.1 s for 21 min (250 frames). The regions used for correlation analysis are outlined. (c) Correlation analysis of relative motion. The correlation of each sequential frame for the regions indicated was calculated for the entire movie; a cell with higher overall motility shows less correlation between frames (see supplemental Experimental Procedures at http://www.jcb.org/cgi/content/full/147/4/743/DC1). Comparative correlation analysis is most precise when the cells are imaged in the same movie as shown in A and B. The graph shows the standard deviation of the average correlation for the entire movie, normalized to the uninjected cell. The shaded regions of the bars indicate the effect of adjusting the threshold of the analysis by ±5 and ±10%; only similar shades should be compared. Error depends on the number of frames analyzed and is <1% in all cases. Bars: (a and b) 5 μm.

difference underlies the segregation of FP-Rab6 or STB from KDELR-FP, endogenous KDELR, and COPI components, and agrees with those of Girod and coworkers (Girod et al., 1999).

FP-Rab6 Trafficking and Shiga Toxin B-Fragment Transport Are Intimately Associated with the Peripheral ER

Since the ER is the final destination of STB retrograde transport, and extends in a network throughout the cell periphery, where active FP-Rab6 trafficking takes place, we observed ER dynamics together with FP-Rab6 or STB in live cells. PtK_2 cells were cotransfected with expression constructs for the ER resident protein CFP-Sec61β, and YFP-Rab6. FP-Sec61β is a fluorescent protein fusion to a component of the machinery that translocates nascent polypeptides into the lumen of the ER (Rolls et al., 1999; Fig. 1 a). FP-Rab6 TCs translocated along the network of the peripheral ER (Fig. 8 a, and supplemental movies at http://www.jcb.org/cgi/content/full/147/4/743/DC1). ER and FP-Rab6 dynamics were intimately related—often an ER tubule extends with FP-Rab6 TC at its tip, or pulses of brighter intensity within the ER network fluctuated synchronously, following behind a moving FP-Rab6 TC (Fig. 8 a and additional movies). Stable domains of FP-Rab6 remained associated with the tips of ER tubules. These associations appear specific to FP-Rab6 TCs, since other microtubule-associated trafficking structures, such as those defined by KDELR-FP, do not display such associations (Fig. 5 and supplemental movies at http://www.jcb.org/cgi/content/full/147/4/743/DC1). FP-Rab6 transport carriers are thus closely associated with the final destination of their cargo.

Corner regions were a distinctive feature of both GFP-Rab6 and STB Golgi→ER transport. The appearance and disappearance of STB accumulation in these regions correlated with the period of maximal initial transport from the Golgi to the ER; they appeared after ~15 min of transport and disappeared by 5 h (compare Fig. 4, a and c). This correlation prompted us to further define the relationship between the corner regions and the ER during STB retrograde transport, so we observed STB dynamics in live HeLa cells transiently transfected with GFP-Sec61β. Fig. 8 b shows STB dispersal from a peripheral corner region into the network of the ER. Quantitative image correla-

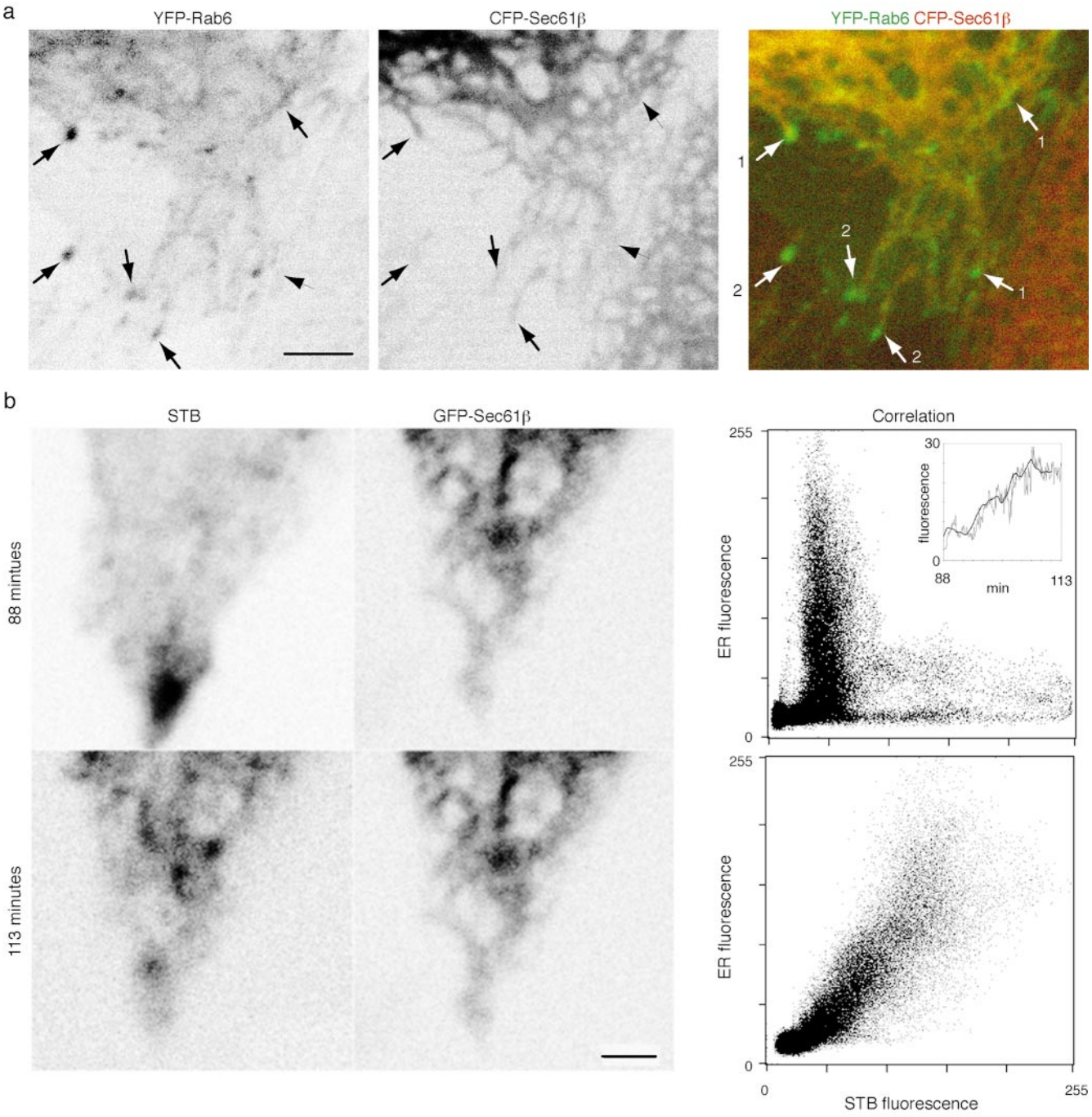

Figure 8. Shiga toxin B-fragment transport, FP-Rab6 trafficking and peripheral ER dynamics. See also the Fig. 8 movies and the Additional Experimental Procedures online at http://www.jcb.org/cgi/content/full/147/4/743/DC1. (a) FP-Rab6 traffics along the peripheral ER and stably associates with the tips of ER tubules. YFP-Rab6 and CFP-Sec61β were coexpressed in a PtK_2 cell. Shown is one time point from a movie covering 16 min (images acquired every 7.6 s) of a cell corner region. Arrows show FP-Rab6 TCs along the ER network (1) and stably associated with tips of ER tubules (2). (b) Shiga toxin B-fragment enters the ER from peripheral corner regions. Dispersal of STB accumulated in a peripheral corner regions was imaged for 20 min after STB was internalized 90 min at 37°C in a HeLa cell expressing the ER resident GFP-Sec61β. Images were acquired every 6.1 s. Shown are initial and final images of STB dispersal, and the correlation plots of STB and the ER at each time. Bars, 4 μm.

tion analysis shows that STB and GFP-Sec61β are initially separate, and increasingly colocalize as STB adopts the pattern of the ER network over time (Fig. 8 b and supplemental movies at http://www.jcb.org/cgi/content/full/147/4/743/DC1). Relative STB levels in the ER increase 22-fold comparing the first and last frame of the movie (Fig. 8 b), and the general trend shows a fivefold increase over time (Fig. 8 b, inset). The correlation between STB and the ER images at the later times are comparable to images of two different antibodies staining the same structure

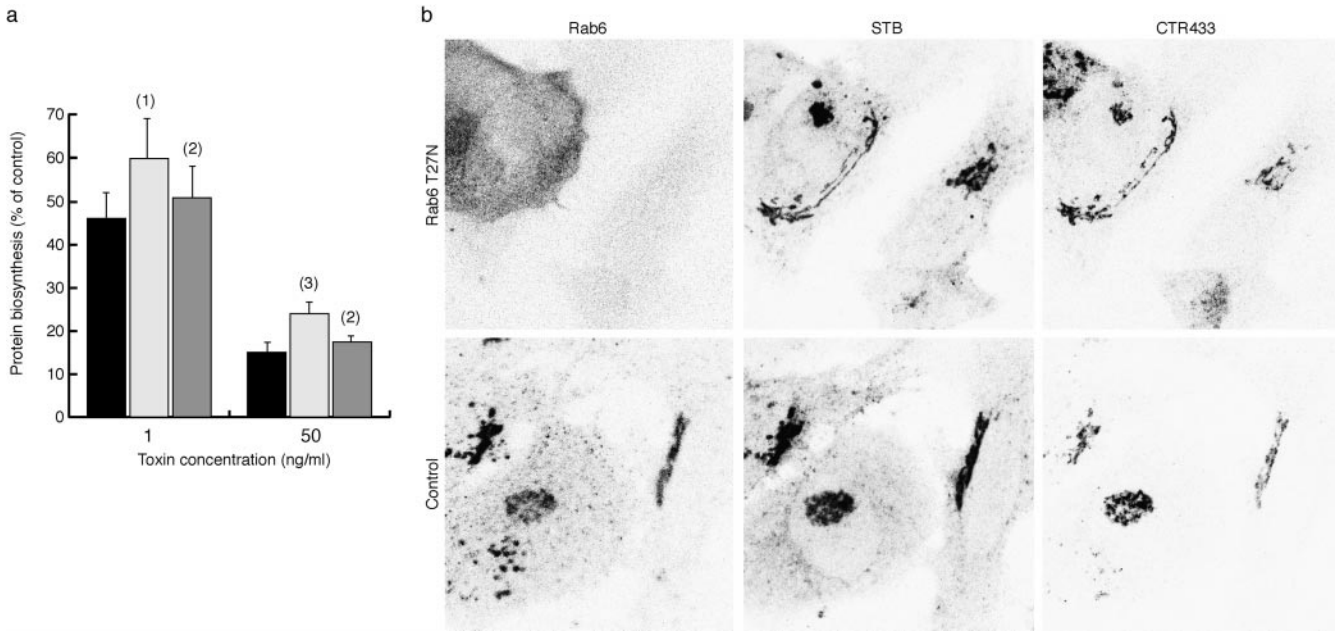

Figure 9. Overexpression of Rab6 T27N inhibits Golgi→ER transport of Shiga holotoxin. (a) Toxicity of Shiga holotoxin is reduced in cells overexpressing Rab6T27N. HeLa cells were mock transfected (dark grey) or transfected with Rab6T27N (light grey) or Rab6I46E (medium grey). After 6 h, Shiga toxin was added at the indicated concentrations and protein biosynthesis was determined as described in Materials and Methods. The data (mean ± SEM, five independent experiments) are presented as percentage of protein biosynthesis in toxin-treated cells compared with non–toxin-treated cells in the same condition. (1) $P < 0.05$, (2) nonsignificant, (3) $P < 0.005$ (paired Student's *t* test). Rab6T27N overexpressing cells were partially protected against Shiga toxin, when compared with control cells. (b) Overexpression of Rab6 T27N does not significantly affect earlier stages of STB transport or Golgi morphology. HeLa cells were mock transfected (control) or transfected with Rab6T27N (T27N) for 12 h. Cy3-labeled B-fragment (STB) was then bound to these cells on ice, the cells were shifted to 37°C for 1 h, then fixed and stained with CTR433 and anti-Rab6 antibodies. In cells overexpressing Rab6T27N (identified by high Rab6 cytoplasmic staining), confocal microscopy shows the Golgi is intact and accumulates STB identically to mock transfected or control cells.

(not shown). Peripheral corner regions are thus sites of concentrated ER entry.

Rab6 T27N Inhibits Toxicity of Shiga Holotoxin

Shiga holotoxin transfers from the ER to the cytosol where it inactivates ribosomes through a specific modification of 28S rRNA (Pelham, 1992; Lord and Roberts, 1998a). Toxicity is thus dependent on ER arrival of the toxin, presumably mediated by STB. To ascertain whether Rab6 regulates Golgi→ER transport, we examined the effect of the Rab6 T27N mutant on toxicity of Shiga toxin. Rab6T27N has a strongly reduced affinity for GTP and is thus at steady state preferentially in the GDP-bound conformation. Corresponding Rab protein mutants have dominant negative effect in several experimental systems (Tisdale et al., 1992; Riederer et al., 1994; Stenmark et al., 1994). Overexpression of Rab6T27N with the T7 vaccinia system (Martinez et al., 1994; for review see Stenmark et al., 1995) significantly reduced Shiga toxin-induced inhibition of protein biosynthesis in HeLa cells (Fig. 9 a). Overexpression of a Rab6 mutant with a mutation in its effector loop (Rab6I46E) had no effect on toxicity (Fig. 9 a). Scatchard analysis on cells that were transfected for 6 h showed that compared with mock transfected cells, Rab6T27N overexpressing cells had the same number of binding sites for STB (0.79×10^6 versus 0.78×10^6 sites/cell, respectively), and that STB affinity for its receptor globotriaosyl ceramide was the same in both conditions (0.135 and 0.103 μM, respectively). STB transport to the Golgi was not significantly altered in cells overexpressing Rab6T27N for 6 (not shown) or even 12 h (Fig. 9 b), and costaining for the Golgi marker CTR433 (Martinez et al., 1997) shows overall Golgi morphology is intact, indicating that inhibition of toxicity is due to specific impairment of a Golgi→ER transport step. Together, these results suggest that native Rab6 regulates the FP-Rab6/STB Golgi→ER transport pathway.

Discussion

Our results are consistent with the idea that the FP-Rab6 membrane system defines a separate compartment that corresponds to a Golgi→ER transport pathway containing specific retrograde cargo and exhibiting distinct functional requirements. The FP-Rab6 compartment comprises all FP-Rab6 elements, the Golgi-associated pool, tubular and globular trafficking elements, and peripheral corner regions. It is separate from some of the traditionally defined morphological compartments (endosomes, lysosomes, and Golgi→plasma membrane transport carriers), and partly overlaps with others (Golgi, ER). FP-Rab6 dynamics in live cells emphasized elements that were neglected in static images, thus revealing morphological features of endogenous Rab6 that

had previously been overlooked (Goud et al., 1990; Antony et al., 1992). Since endogenous Rab6 and FP-Rab6 have common features (Fig. 2), FP-Rab6 dynamics are most likely not induced by overexpression of the FP-Rab6 fusion protein.

During the period when STB underwent transport from the Golgi to the ER, it accumulated in FP-Rab6 trafficking structures and together with FP-Rab6 in distinctive corner regions. At later times, when the STB has been shown to cycle between the ER and Golgi (Johannes et al., 1997), it continued to traffic in FP-Rab6 elements, although to a lesser extent. These observations indicate that FP-Rab6 trafficking elements are retrograde TCs, and are consistent with the idea that the initial vectorial pulse of STB transport concentrates it in FP-Rab6 retrograde carriers, resulting in strong coincidence at early times. At later times, as STB partitions between the Golgi and ER and begins cycling, only a proportion undergoes Golgi→ER retrograde transport during a given period, resulting in weaker coincidence. Since STB and FP-Rab6 trafficking behavior can be observed independently, it is unlikely that one or the other induces the transport carriers, and further support the ideas that FP-Rab6 does not induce trafficking elements, and that STB uses a preexisting cellular pathway.

The coincidence of FP-Rab6 and STB in distinctive peripheral corner regions prompted us to investigate these regions further. STB dissipated into the ER network directly from these regions, indicating that they are ER entrance sites (Fig. 8 b, and supplemental movies at http://www.jcb.org/cgi/content/full/147/4/743/DC1). We cannot exclude that STB entered the ER at other locations or along the entire ER network; we conclude only that ER entrance from the corner regions was particularly pronounced. Other transport steps are also concentrated at specialized sites: ER exit occurs in specialized regions that recruit COPII coat proteins to the membrane to concentrate and sort anterograde cargo from the ER (Balch et al., 1994; Bannykh et al., 1996; Presley et al., 1997; Scales et al., 1997), and delivery of secretory cargo also appears to be directed to a specialized area of the plasma membrane, a targeting patch, in both yeast and polarized mammalian cells (Finger and Novick, 1998; Grindstaff et al., 1998).

STB traverses endosomes before it arrives in the Golgi (Mallard et al., 1998), so it remained possible that the STB which coincided with FP-Rab6 trafficking elements was in endosomes. This is, however, highly unlikely since we observed STB in FP-Rab6 trafficking structures long after the bulk of STB had exited endosomal structures (after 5 h at 37°C), and since STB blocked in the endosomes at 19.5°C did not coincide with FP-Rab6 (not shown). Consistent with this, FP-Rab6 peripheral elements never colocalized with a number of different endosomal markers, including transferrin receptor and FP-Rab5 in fixed cells, and labeled transferrin in live cells (continuous uptake; not shown). It is also highly unlikely that FP-Rab6 trafficking elements represent TCs containing post-Golgi anterograde cargo, despite superficial similarities (Hirschberg et al., 1998; Toomre et al., 1999). When imaged in live cells, Golgi-to-plasma membrane TCs, revealed by four separate FP markers, exhibited different behavior, trafficked to different regions of the cell, and did not coincide in live cell double-labeling experiments (White, J., unpublished observations).

Since FP-Rab6 coincided with a retrograde cargo during Golgi→ER transport, we expected FP-Rab6 TCs to coincide with proteins involved in retrieval of ER residents. This was, however, not the case. FP-Rab6 was separate from KDELR-FP in live cells, and COPI components and endogenous KDELR in fixed cells. Consistent with this, STB segregated away from KDELR-FP in live cells; we observed no coincidence at early times of STB transport, and only partial coincidence from 2 to 5 h. Even when both proteins were in the ER network, they excluded one another, appearing as separate domains within the ER network. These results indicate that STB traffics predominantly in the FP-Rab6 pathway. The partial coincidence of STB and KDELR-FP-positive structures may be due to specific retrograde transport in these structures, or may be mis-sorting into this pathway at higher STB levels. Since KDELR-FP cycles between the ER and the Golgi, a subset of KDELR-FP trafficking may represent an anterograde transport step, leading to the additional possibility that STB cycles to the Golgi in anterograde structures that contain KDELR-FP, and to the ER in FP-Rab6 structures.

The differences between ER retrieval and FP-Rab6/STB retrograde transport extend to the functional level. Previous studies indicate toxin proteins define two functionally different retrograde pathways to the ER. Jackson and coworkers have shown some toxin proteins require the KDEL-retrieval system for efficient transport to the ER, while others do not (Jackson et al., 1999). Girod and coworkers have recently shown that microinjection of anti-EAGE antibodies, potent inhibitors of COPI function in live cells (Pepperkok et al., 1993, 1998) inhibits Golgi→ER transport of toxin proteins which contain KDEL-like motifs. In contrast, transport of STB, and likewise the holotoxin, is unaffected (Girod, A., B. Storrie, J.C. Simpson, J.M. Lord, T. Nilsson, and R. Pepperkok, manuscript submitted for publication). Here, we show that FP-Rab6 trafficking is not inhibited by anti-EAGE microinjection, but KDELR-FP trafficking is reduced to 60% of control (Fig. 7). These results are consistent with the observation that modified STB reach the ER equally well with or without a KDEL retrieval signal. They also imply that trafficking is linked to transport of KDELR (and presumably other components of the ER retrieval system), a relationship that is often assumed but which has not been shown. It was previously unclear whether the toxin protein pathway was preexisting or a consequence of the toxin itself, but the coincidence of FP-Rab6 and STB in trafficking structures with the same functional characteristic strongly argues that STB uses a COPI-independent cellular pathway defined by FP-Rab6.

Our results suggest native Rab6 regulates this alternate Golgi→ER transport pathway. In previous studies, high overexpression of active forms of Rab6 (Q72L mutant or wild-type) stimulated retrograde transport from the Golgi to the ER, progressively relocating Golgi residents to the ER and indirectly inhibiting intra-Golgi anterograde transport (Martinez et al., 1994, 1997). This interpretation fits well with the general idea that Rab proteins are active in their GTP-bound form (Novick and Zerial, 1997). Consistent with these observations, overexpression of

Rab6:GDP (T27N) reduces toxicity of the holotoxin by inhibiting a Golgi→ER transport step (Fig. 9), without altering earlier transport steps or overall Golgi morphology. We note that overexpression of active forms of Rab6 does not in fact stimulate ER arrival of STB, because STB must be transported to the ER via an intact Golgi structure (Johannes et al., 1997), and upon overexpression of active Rab6 the Golgi redistributes to the ER and is no longer intact (Martinez et al., 1997). Taken together, these results imply that this pathway is activated by GTP-Rab6 and inhibited by GDP-Rab6.

Why would an alternate Golgi→ER pathway exist? Presumably it would be used by a subset of cellular components, not only by toxin proteins. Supporting this, verotoxin and Shiga-like toxins have homology to cellular proteins that are transported from the cell surface to the nuclear envelope, a subdomain of the ER (Lingwood and Yiu, 1992; Maloney and Lingwood, 1994; Khine et al., 1998). These components do not have a recognizable ER retrieval motif, yet appear to reach the ER. Other cellular components that return to the ER also lack a retrieval motif. Resident Golgi proteins slowly but continuously cycle through the ER (Cole, 1998), apparently via COPI-independent mechanisms (Girod et al., 1999). A transport pathway to the ER could be used for degradation of transmembrane proteins: certain transmembrane ER proteins may be extracted from the membrane by retrotranslocation to be targeted for proteasome-mediated degradation in the cytosol (Ward et al., 1995; Kopito, 1997; Plemper et al., 1997). Transmembrane proteins from other intracellular compartments could also undergo ER-based degradation. Another rationale for an alternate pathway would be a mechanism to recycle lipid components to the ER. Intracellular lipid trafficking is not yet well characterized, but it is notable that STB binds a glycolipid receptor, globotriaosyl ceramide, at the cell surface (Cohen et al., 1987). It remains to be shown whether STB follows its glycolipid receptor as far as the ER.

The idea that Rab proteins define trafficking routes within the cell was proposed based primarily on the apparent specificity of their localization (Simons and Zerial, 1993), but until this study has never been directly tested. Observation of Rab protein dynamics provides even further insight than simple localization: Previous studies localized native Rab6 to the Golgi (Goud et al., 1990; Antony et al., 1992), but its cellular function there was unclear (Martinez et al., 1994, 1997). Observation of FP-Rab6 TCs and the accumulation of a specific retrograde cargo within them during Golgi→ER transport directly indicate a role for Rab6 in transport to the ER. Furthermore, microtubule-dependent translocation of FP-Rab6 TCs rationalizes the direct association of Rab6:GTP with Rabkinesin-6 (Echard et al., 1998). Our studies of FP-Rab6 dynamics in live cells provide the cellular context in which to interpret the function of Rab6 at the molecular level.

The authors gratefully thank Pascal Stein and Melissa Rolls for FP-Sec61β and other ER FPs; Roger Tsien for ECFP plasmid; Ann Atzberger for cell sorting; Rainer Saffrich for help with microinjections; Rainer Pepperkok and Ken Sawin for antibodies; Joachim Füllekrug, Birte Sönnichsen, and Anja Habermann for EM; Melissa Rolls, Freddy Frischknecht, Eric Karsenti, and Marino Zerial for discussions and critical comments on the manuscript; Jim Swoger for assistance with optics; and the CCC development team: Stephan Albrecht (DSP programming), Alfons Riedinger (software design and programming), Georg Ritter (digital hardware), Nick Salmon (software design and programming), Thomas Stefany (optics), and Reiner Stricker (analogue hardware).

L. Johannes and B. Goud were supported by grants from the European Union (ERB FMRX CT 96-0020), the Human Frontier Science Program, the Association de la Recherche contre le Cancer, and the Ligue Nationale contre le Cancer.

Submitted: 27 July 1999
Revised: 5 October 1999
Accepted: 5 October 1999

References

Antony, C., C. Cibert, G. Geraud, A. Santa Maria, B. Maro, V. Mayau, and B. Goud. 1992. The small GTP-binding protein rab6p is distributed from medial Golgi to the trans-Golgi network as determined by a confocal microscopic approach. *J. Cell Sci.* 103:785–796.

Aoe, T., E. Cukierman, A. Lee, D. Cassel, P.J. Peters, and V.W. Hsu. 1997. The KDEL receptor, ERD2, regulates intracellular traffic by recruiting a GTPase-activating protein for ARF1. *EMBO (Eur. Mol. Biol. Organ.) J.* 16: 7305–7316.

Balch, W.E., J.M. McCaffery, H. Plutner, and M.G. Farquhar. 1994. Vesicular stomatitis virus glycoprotein is sorted and concentrated during export from the endoplasmic reticulum. *Cell.* 76:841–852.

Bannykh, S.I., T. Rowe, and W.E. Balch. 1996. The organization of endoplasmic reticulum export complexes. *J. Cell Biol.* 135:19–35.

Cohen, A., G.E. Hannigan, B.R. Williams, and C.A. Lingwood. 1987. Roles of globotriaosyl- and galabiosylceramide in verotoxin binding and high affinity interferon receptor. *J. Biol. Chem.* 262:17088–17091.

Cole, N.B., J. Ellenberg, J. Song, D. DiEuliis, and J. Lippincott-Schwartz. 1998. Retrograde transport of Golgi-localized proteins to the ER. *J. Cell Biol.* 140: 1–15.

Cosson, P., and F. Letourneur. 1994. Coatomer interaction with di-lysine endoplasmic reticulum retention motifs. *Science* 263:1629–1631.

Cosson, P., and F. Letourneur. 1997. Coatomer (COPI)-coated vesicles: role in intracellular transport and protein sorting. *Curr. Opin. Cell Biol.* 9:484–487.

Dominguez, M., K. Dejgaard, J. Füllekrug, S. Dahan, A. Fazel, J.P. Paccaud, D.Y. Thomas, J.J. Bergeron, and T. Nilsson. 1998. gp25L/emp24/p24 protein family members of the cis-Golgi network bind both COP I and II coatomer. *J. Cell Biol.* 140:751–765.

Duden, R., G. Griffiths, R. Frank, P. Argos, and T.E. Kreis. 1991. β-COP, a 110 kd protein associated with non-clathrin-coated vesicles and the Golgi complex, shows homology to β-adaptin. *Cell.* 64:649–665.

Echard, A., F. Jollivet, O. Martinez, J.J. Lacapere, A. Rousselet, I. Janoueix-Lerosey, and B. Goud. 1998. Interaction of a Golgi-associated kinesin-like protein with Rab6. *Science* 279:580–585.

Ellenberg, J., J. Lippincott-Schwartz, and J.F. Presley. 1998. Two-color green fluorescent protein time-lapse imaging. *Biotechniques.* 25:838–842, 844–846.

Finger, F.P., and P. Novick. 1998. Spatial regulation of exocytosis: lessons from yeast. *J. Cell Biol.* 142:609–612.

Fuerst, T.R., E.G. Niles, F.W. Studier, and B. Moss. 1986. Eukaryotic transient-expression system based on recombinant vaccinia virus that synthesizes bacteriophage T7 RNA polymerase. *Proc. Natl. Acad. Sci. USA.* 83:8122–8126.

Füllekrug, J., T. Suganuma, B.L. Tang, W. Hong, B. Storrie, and T. Nilsson. 1999. Localization and recycling of gp27 (hp24γ3): complex formation with other p24 family members. *Mol. Biol. Cell.* 10:1939–1955.

Girod, A., B. Storrie, J.C. Simpson, L. Johannes, B. Goud, L.M. Roberts, J.M. Lord, T. Nilsson, and R. Pepperkok. 1999. Evidence for a COPI-independent transport route from the Golgi complex to the endoplasmic reticulum. *Nat. Cell Biol.* 1:423–430.

Goud, B., A. Zahraoui, A. Tavitian, and J. Saraste. 1990. Small GTP-binding protein associated with Golgi cisternae. *Nature.* 345:553–556.

Grindstaff, K.K., C. Yeaman, N. Anandasabapathy, S.C. Hsu, E. Rodriguez-Boulan, R.H. Scheller, and W.J. Nelson. 1998. Sec6/8 complex is recruited to cell-cell contacts and specifies transport vesicle delivery to the basal-lateral membrane in epithelial cells. *Cell.* 93:731–740.

Heim, R., D.C. Prasher, and R.Y. Tsien. 1994. Wavelength mutations and post-translational autoxidation of green fluorescent protein. *Proc. Natl. Acad. Sci. USA.* 91:12501–12504.

Heim, R., A.B. Cubitt, and R.Y. Tsien. 1995. Improved green fluorescence. *Nature.* 373:663–664.

Heim, R., and R.Y. Tsien. 1996. Engineering green fluorescent protein for improved brightness, longer wavelengths and fluorescence resonance energy transfer. *Curr. Biol.* 6:178–182.

Hirschberg, K., C.M. Miller, J. Ellenberg, J.F. Presley, E.D. Siggia, R.D. Phair, and J. Lippincott-Schwartz. 1998. Kinetic analysis of secretory protein traffic and characterization of Golgi to plasma membrane transport intermediates in living cells. *J. Cell Biol.* 143:1485–1503.

Jackson, M.R., T. Nilsson, and P.A. Peterson. 1990. Identification of a consensus motif for retention of transmembrane proteins in the endoplasmic reticu-

lum. *EMBO (Eur. Mol. Biol. Organ.) J.* 9:3153–3162.
Jackson, M.E., J.C. Simpson, A. Girod, R. Pepperkok, L.M. Roberts, and J.M. Lord. 1999. The KDEL retrieval system is exploited by Pseudomonas exotoxin A, but not by Shiga-like toxin-1, during retrograde transport from the Golgi complex to the endoplasmic reticulum. *J. Cell Sci.* 112:467–475.
Johannes, L., and B. Goud. 1998. Surfing on a retrograde wave: how does Shiga toxin reach the endoplasmic reticulum? *Trends Cell Biol.* 8:158–162.
Johannes, L., D. Tenza, C. Antony, and B. Goud. 1997. Retrograde transport of KDEL-bearing B-fragment of Shiga toxin. *J. Biol. Chem.* 272:19554–19561.
Khine, A.A., M. Firtel, and C.A. Lingwood. 1998. CD77-dependent retrograde transport of CD19 to the nuclear membrane: functional relationship between CD77 and CD19 during germinal center B-cell apoptosis. *J. Cell Physiol.* 176:281–292.
Kopito, R.R. 1997. ER quality control: the cytoplasmic connection. *Cell.* 88: 427–430.
Le Bot, N., C. Antony, J. White, E. Karsenti, and I. Vernos. 1998. Role of Xklp3, a subunit of the *Xenopus* kinesin II heterotrimeric complex, in membrane transport between the endoplasmic reticulum and the Golgi apparatus. *J. Cell Biol.* 143:1559–1573.
Letourneur, F., E.C. Gaynor, S. Hennecke, C. Demolliere, R. Duden, S.D. Emr, H. Riezman, and P. Cosson. 1994. Coatomer is essential for retrieval of dilysine-tagged proteins to the endoplasmic reticulum. *Cell.* 79:1199–1207.
Lingwood, C.A., and S.K. Yiu. 1992. Glycolipid modification of alpha 2 interferon binding. Sequence similarity between the alpha 2 interferon receptor and verotoxin (Shiga-like toxin) B-subunit. *Biochem. J.* 283:25–26.
Linstedt, A.D., and H.P. Hauri. 1993. Giantin, a novel conserved Golgi membrane protein containing a cytoplasmic domain of at least 350 kDa. *Mol. Biol. Cell.* 4:679–693.
Llorente, A., A. Rapak, S.L. Schmid, B. van Deurs, and K. Sandvig. 1998. Expression of mutant dynamin inhibits toxicity and transport of endocytosed ricin to the Golgi apparatus. *J. Cell Biol.* 140:553–563.
Lord, J.M., and L.M. Roberts. 1998. Toxin entry: retrograde transport through the secretory pathway. *J. Cell Biol.* 140:733–736.
Louvard, D., H. Reggio, and G. Warren. 1982. Antibodies to the Golgi complex and the rough endoplasmic reticulum. *J. Cell Biol.* 92:92–107.
Majoul, I.V., P.I. Bastiaens, and H.D. Soling. 1996. Transport of an external Lys-Asp-Glu-Leu (KDEL) protein from the plasma membrane to the endoplasmic reticulum: studies with cholera toxin in Vero cells. *J. Cell Biol.* 133: 777–789.
Majoul, I., K. Sohn, F.T. Wieland, R. Pepperkok, M. Pizza, J. Hillemann, and H.D. Soling. 1998. KDEL receptor (Erd2p)-mediated retrograde transport of the cholera toxin A subunit from the Golgi involves COPI, p23, and the COOH terminus of Erd2p. *J. Cell Biol.* 143:601–612.
Mallard, F., C. Antony, D. Tenza, J. Salamero, B. Goud, and L. Johannes. 1998. Direct pathway from early/recycling endosomes to the Golgi apparatus revealed through the study of Shiga toxin B-fragment transport. *J. Cell Biol.* 143:973–990.
Maloney, M.D., and C.A. Lingwood. 1994. CD19 has a potential CD77 (globotriaosyl ceramide)-binding site with sequence similarity to verotoxin B-subunits: implications of molecular mimicry for B cell adhesion and enterohemorrhagic *Escherichia coli* pathogenesis. *J. Exp. Med.* 180:191–201.
Martinez, O., and B. Goud. 1998. Rab proteins. *Biochim. Biophys. Acta.* 1404: 101–112.
Martinez, O., A. Schmidt, J. Salamero, B. Hoflack, M. Roa, and B. Goud. 1994. The small GTP-binding protein rab6 functions in intra-Golgi transport. *J. Cell Biol.* 127:1575–1588.
Martinez, O., C. Antony, G. Pehau-Arnaudet, E.G. Berger, J. Salamero, and B. Goud. 1997. GTP-bound forms of rab6 induce the redistribution of Golgi proteins into the endoplasmic reticulum. *Proc. Natl. Acad. Sci. USA.* 94: 1828–1833.
Miyawaki, A., J. Llopis, R. Heim, J.M. McCaffery, J.A. Adams, M. Ikura, and R.Y. Tsien. 1997. Fluorescent indicators for Ca2+ based on green fluorescent proteins and calmodulin. *Nature.* 388:882–887.
Munro, S., and H.R. Pelham. 1987. A C-terminal signal prevents secretion of luminal ER proteins. *Cell.* 48:899–907.
Nilsson, T., M. Pypaert, M.H. Hoe, P. Slusarewicz, E.G. Berger, and G. Warren. 1993. Overlapping distribution of two glycosyltransferases in the Golgi apparatus of HeLa cells. *J. Cell Biol.* 120:5–13.
Novick, P., and M. Zerial. 1997. The diversity of Rab proteins in vesicle transport. *Curr. Opin. Cell Biol.* 9:496–504.
Pääbo, S., F. Weber, T. Nilsson, W. Schaffner, and P.A. Peterson. 1986. Structural and functional dissection of an MHC class I antigen-binding adenovirus glycoprotein. *EMBO (Eur. Mol. Biol. Organ.) J.* 5:1921–1927.
Palmer, D.J., J.B. Helms, C.J. Beckers, L. Orci, and J.E. Rothman. 1993. Binding of coatomer to Golgi membranes requires ADP-ribosylation factor. *J. Biol. Chem.* 268:12083–12089.
Pelham, H.R. 1988. Evidence that luminal ER proteins are sorted from secreted proteins in a post-ER compartment. *EMBO (Eur. Mol. Biol. Organ.) J.* 7:913–918.
Pelham, H.R. 1991. Recycling of proteins between the endoplasmic reticulum and Golgi complex. *Curr. Opin. Cell Biol.* 3:585–591.
Pelham, H.R. 1992. The Florey Lecture, 1992. The secretion of proteins by cells. *Proc. R Soc. Lond. B Biol. Sci.* 250:1–10.
Pepperkok, R., J. Scheel, H. Horstmann, H.P. Hauri, G. Griffiths, and T.E. Kreis. 1993. Beta-COP is essential for biosynthetic membrane transport from the endoplasmic reticulum to the Golgi complex in vivo. *Cell.* 74:71–82.
Pepperkok, R., M. Lowe, B. Burke, and T.E. Kreis. 1998. Three distinct steps in transport of vesicular stomatitis virus glycoprotein from the ER to the cell surface in vivo with differential sensitivities to GTPγS. *J. Cell Sci.* 111:1877–1888.
Plemper, R.K., S. Bohmler, J. Bordallo, T. Sommer, and D.H. Wolf. 1997. Mutant analysis links the translocon and BiP to retrograde protein transport for ER degradation. *Nature.* 388:891–895.
Presley, J.F., N.B. Cole, T.A. Schroer, K. Hirschberg, K.J. Zaal, and J. Lippincott-Schwartz. 1997. ER-to-Golgi transport visualized in living cells. *Nature.* 389:81–85.
Riederer, M.A., T. Soldati, A.D. Shapiro, J. Lin, and S.R. Pfeffer. 1994. Lysosome biogenesis requires Rab9 function and receptor recycling from endosomes to the trans-Golgi network. *J. Cell Biol.* 125:573–582.
Rolls, M.M., P.A. Stein, S.S. Taylor, E. Ha, F. McKeon, and T.A. Rapoport. 1999. A visual screen of a GFP-fusion library identifies a new type of nuclear envelope membrane protein. *J. Cell Biol.* 146:29–44.
Röttger, S., J. White, H.H. Wandall, J.C. Olivo, A. Stark, E.P. Bennett, C. Whitehouse, E.G. Berger, H. Clausen, and T. Nilsson. 1998. Localization of three human polypeptide GalNAc-transferases in HeLa cells suggests initiation of O-linked glycosylation throughout the Golgi apparatus. *J. Cell Sci.* 111:45–60.
Sandvig, K., and B. van Deurs. 1996. Endocytosis, intracellular transport, and cytotoxic action of Shiga toxin and ricin. *Physiol. Rev.* 76:949–966.
Sandvig, K., O. Garred, K. Prydz, J.V. Kozlov, S.H. Hansen, and B. van Deurs. 1992. Retrograde transport of endocytosed Shiga toxin to the endoplasmic reticulum. *Nature.* 358:510–512.
Sandvig, K., M. Ryd, O. Garred, E. Schweda, P.K. Holm, and B. van Deurs. 1994. Retrograde transport from the Golgi complex to the ER of both Shiga toxin and the nontoxic Shiga B-fragment is regulated by butyric acid and cAMP. *J. Cell Biol.* 126:53–64.
Scales, S.J., R. Pepperkok, and T.E. Kreis. 1997. Visualization of ER-to-Golgi transport in living cells reveals a sequential mode of action for COPII and COPI. *Cell.* 90:1137–1148.
Schröder-Köhne, S., F. Letourneur, and H. Riezman. 1998. α-COP can discriminate between distinct, functional di-lysine signals in vitro and regulates access into retrograde transport. *J. Cell Sci.* 111:3459–3470.
Schutze, M.P., P.A. Peterson, and M.R. Jackson. 1994. An N-terminal double-arginine motif maintains type II membrane proteins in the endoplasmic reticulum. *EMBO (Eur. Mol. Biol. Organ.) J.* 13:1696–1705.
Shima, D.T., K. Haldar, R. Pepperkok, R. Watson, and G. Warren. 1997. Partitioning of the Golgi apparatus during mitosis in living HeLa cells. *J. Cell Biol.* 137:1211–1228.
Simons, K., and M. Zerial. 1993. Rab proteins and the road maps for intracellular transport. *Neuron.* 11:789–799.
Sohn, K., L. Orci, M. Ravazzola, M. Amherdt, M. Bremser, F. Lottspeich, K. Fiedler, J.B. Helms, and F.T. Wieland. 1996. A major transmembrane protein of Golgi-derived COPI-coated vesicles involved in coatomer binding. *J. Cell Biol.* 135:1239–1248.
Stamnes, M.A., M.W. Craighead, M.H. Hoe, N. Lampen, S. Geromanos, P. Tempst, and J.E. Rothman. 1995. An integral membrane component of coatomer-coated transport vesicles defines a family of proteins involved in budding. *Proc. Natl. Acad. Sci. USA.* 92:8011–8015.
Stenmark, H., R.G. Parton, O. Steele-Mortimer, A. Lutcke, J. Gruenberg, and M. Zerial. 1994. Inhibition of rab5 GTPase activity stimulates membrane fusion in endocytosis. *EMBO (Eur. Mol. Biol. Organ.) J.* 13:1287–1296.
Stenmark, H., C. Bucci, and M. Zerial. 1995. Expression of Rab GTPases using recombinant vaccinia viruses. *Methods Enzymol.* 257:155–164.
Su, G.F., H.N. Brahmbhatt, J. Wehland, M. Rohde, and K.N. Timmis. 1992. Construction of stable LamB-Shiga toxin B subunit hybrids: analysis of expression in *Salmonella typhimurium* aroA strains and stimulation of B subunit-specific mucosal and serum antibody responses. *Infect. Immunol.* 60: 3345–3359.
Tisdale, E.J., J.R. Bourne, R. Khosravi-Far, C.J. Der, and W.E. Balch. 1992. GTP-binding mutants of rab1 and rab2 are potent inhibitors of vesicular transport from the endoplasmic reticulum to the Golgi complex. *J. Cell Biol.* 119:749–761.
Toomre, D., P. Keller, J. White, J.-C. Olivo, and K. Simons. 1999. Dual-color visualization of *trans*-Golgi network to plasma membrane traffic along microtubules in living cells. *J. Cell Sci.* 112:21–33.
Ward, C.L., S. Omura, and R.R. Kopito. 1995. Degradation of CFTR by the ubiquitin-proteasome pathway. *Cell.* 83:121–127.
White, J., B. Storrie, S. Rötger, E.H.K. Stelzer, T. Suganuma, and T. Nilsson. 1998. Recycling of Golgi resident glycosyltransferases through the ER reveals a novel pathway and provides an explanation for nocodazole-induced Golgi scattering. *J. Cell Biol.* 143:1505–1521.